Fluorescence Lifetime Imaging Microscopy: Advancing the Frontier of Material Science

Fariyad Ali,[a‡*] Subhankar Kundu[b‡*]

[a]Department of Chemistry, Iowa State University, 1605 Gilman Hall, Ames, Iowa, 50011.

[b]Research Division, Hoxworth Blood Center, College of Medicine, UC Health, University of Cincinnati, 3130 Highland Ave, Cincinnati, Ohio 45219.

Fluorescence Lifetime Imaging Microscopy, Single Photon Emission, Nanomaterials, Molecular Self-assembly, Polymers, Metal-Organic Frameworks

ABSTRACT: Controlling the formation dynamics and tuning the micro/nanoscale structures are crucial to design materials with desired properties for specific applications. Thus, the visualization of the structures and probing of the *in situ* formation mechanisms of molecular materials is quite important albeit challenging. Recently, fluorescence lifetime imaging microscopy (FLIM) has emerged as a valuable complementary, robust, and non-invasive technique along with conventional imaging tools to unravel the nanoscale morphology and dynamics of fluorescent or fluorophore-tagged molecular materials. Considering the current need to understand the field, this perspective article emphasizes the growing importance of FLIM to explore the salient aspects of diverse materials, including semiconductor nanocrystals, molecular self-assembly, polymers, and metal-organic frameworks. We will deliberate the fundamental features of FLIM and its applications to decipher the stimuli-responsive dynamic molecular self-assembly process, the growth kinetics and mechanistic insights of polymers, and probe the phase purity in metal-organic frameworks. We will also highlight the use of FLIM in photoluminescence blinking and photon antibunching which can resolve many unreciprocated facts in the field of semiconductor nanocrystals. Beyond presenting up-to-date knowledge in the field, we will outline the potential future directions of FLIM, emphasizing its role in developing novel materials and improving existing ones. This advancement paves the way for new opportunities in materials science research and applications.

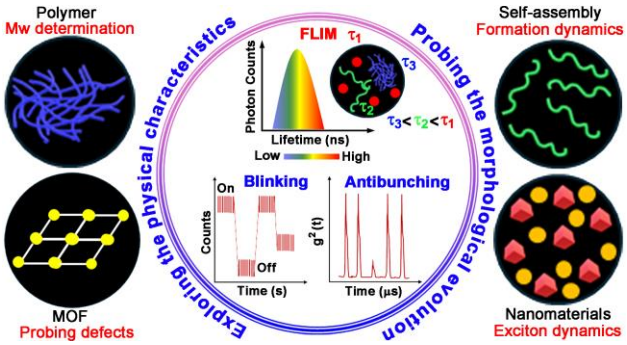

1. INTRODUCTION

Exploring the structure-property relationship of materials has drawn the significant attention of the scientific community because of their applications in optoelectronics, bioimaging, sensing, and catalysis.[1-17] Consequently, significant research efforts have been devoted to design and engineering materials by elucidating the influence of micro- and nanostructures, as well as their formation dynamics, on properties and performance.[18-41] Giri *et al*. demonstrated that hypercrosslinked porous polymers with a nanosheet morphology exhibit superior performance in removing micropollutants from water compared to their spherical nanoparticle counterparts.[42] Zhang *et al*. studied how the shape of amphiphilic perylene bisimide nanoaggregates affects their light-emitting properties, showing the impact of changes in structure on their behavior.[43] Mitra *et al*. showed that covalent organic frameworks with a nanosheet morphology exhibit superior efficacy in drug delivery to cancer cells compared to other morphological forms.[44] Therefore, visualizing the nano- and microscale morphologies of various materials has become essential for understanding their properties and tailoring them for task-specific applications.

Table 1. A relative analysis of the salient features of diverse imaging tools that have been used for the exploration of the properties and functions of different materials.

Techniques	Working principle	Nature of samples	Resolution	Pros	Cons	Ref. no.
FESEM	A focused electron beam scans a sample's surface, and the interactions create signals to form an image	Mostly for solid or dried samples	Typically, 1-2 nm, depending on the sample and operating conditions	(i) Excellent surface resolution (ii) Detailed topographical information	(i) Samples to be conductive and possibly coated (ii) Operates under a vacuum, which can limit the types of samples analyzed (iii) No *in situ* imaging	47, 50, 51
TEM	A beam of electrons passes through a thin sample, revealing its structure through their interactions	Applicable for solid, dried, and frozen specimens	Down to sub-nanometer, with high-resolution TEM (HRTEM) reaching below 0.1 nm	(i) Can resolve the atomic structure of materials (ii) Provides information about the internal structure of samples	(i) Samples must be very thin (typically less than 100 nm) (ii) Requires complex sample preparation and operation (iii) No *in situ* imaging	56-60
AFM	A sharp-tipped cantilever scans a sample's surface, and its deflection creates a topographical map	Works with solid (dried or frozen) samples	Typically, 0.1 nm vertically and a few nanometers laterally	(i) Provides detailed topographical maps at the nanoscale (ii) Can image samples in ambient conditions without damaging them	(i) Slow Scan Speed (ii) Small scanning area compared to optical techniques	62-66
CLSM	Uses point illumination and a pinhole to reject out-of-focus light, enhancing image contrast and optical resolution	Works with solutions, dispersions, solids, and biological samples	Approximately 200 nm laterally and 500-700 nm axially	(i) Allows for imaging of specific focal planes within a specimen (ii) Can be used to construct 3D images of specimens	(i) High-intensity laser light can cause photobleaching (ii) Scan Speed: Slower compared to wide-field microscopy	46, 54
FLIM	Measures how long a fluorophore stays excited before emitting light (fluorescence lifetime), revealing details about the microenvironment	Works with solutions, dispersions, solids, and biological samples	Typically, diffraction-limited, like other optical microscopy techniques (200-300 nm laterally)	(i) Sensitive to the variation of the microenvironment (e.g., polarity, viscosity, pH, ion concentration) (ii) Provides fluorophore concentration-independent data	(i) Requires specialized equipment and expertise (ii) Temporal resolution is Limited by the speed of photon detection (iii) Requires fluorescent or fluorophore-tagged materials	68-73

Over the years, tools like field emission scanning electron microscopy (FESEM), transmission electron microscopy (TEM), atomic force microscopy (AFM), and confocal laser scanning microscopy (CLSM) have been widely used for imaging.[45-55] FESEM provides high-resolution and detailed images of a material's surface.[47,50,51] It is widely used to examine microstructural details which are essential for understanding material properties such as adhesion, conductivity, and mechanical strength.[48,49] TEM offers atomic-level resolution to study the internal structure of materials (Table 1).[56-60] It has been used to analyze crystallographic structures, defects, and interfaces within materials that influence their electronic, optical, and mechanical properties.[53,56,58-60] However, the requirement of drying or freezing samples for both (FESEM and TEM) might alter the natural state and dynamic behaviors of the materials, potentially affecting the authenticity of the observations (Table 1).[46,54] Kundu *et al*. demonstrated how solvent evaporation affects nanoscale morphologies in molecular self-assembly during the sample preparation for electron microscopy.[61] On the other hand, AFM is used to check the surface topography and mechanical properties at the nanoscale.[62-64] However, the interaction between the AFM tip and the sample can significantly influence the imaging results.[65,66] Shen *et al*. demonstrated that the artifacts obtained in the morphology of sapphire cylinder protrusions were due to the influence of AFM tips.[67] CLSM is used for optical sectioning and 3D reconstruction of specimens. It is particularly useful for studying fluorescent or fluorophore-tagged biological samples, polymers, and composite materials.[46] However, the high

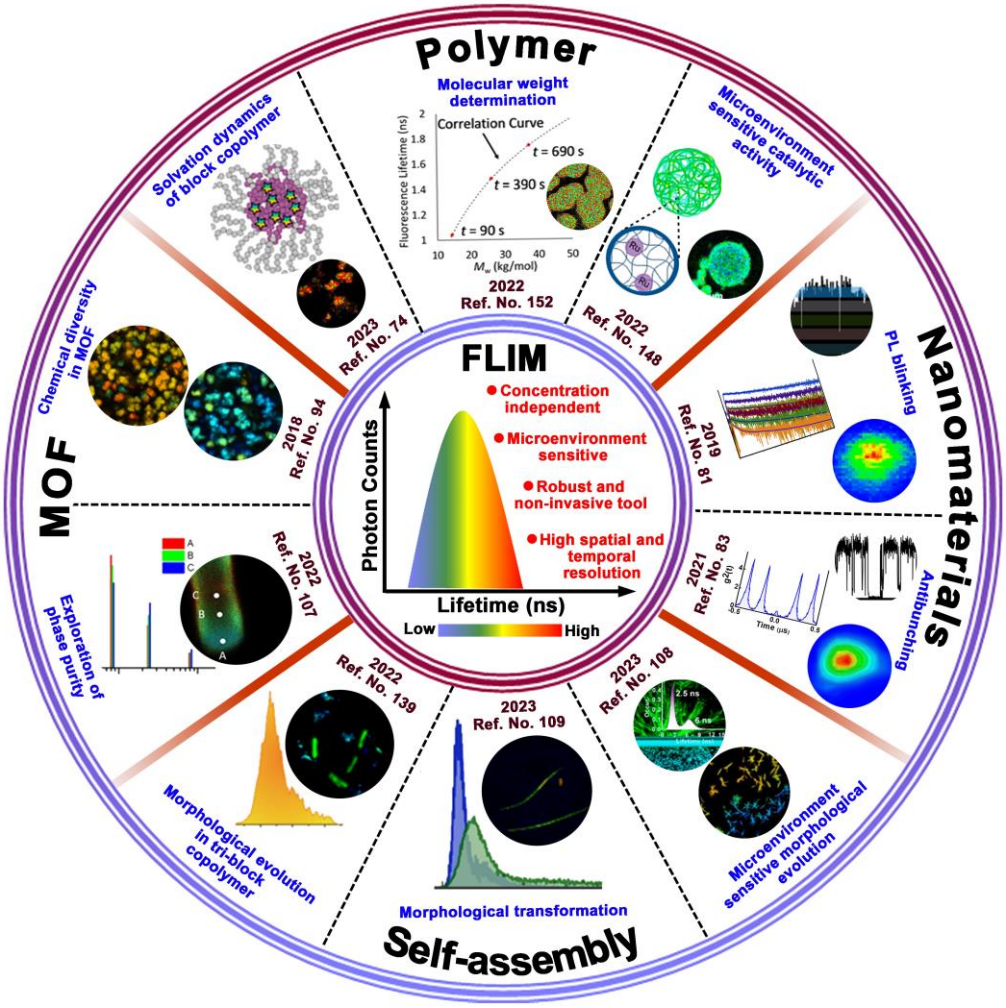

Figure 1. Schematic illustration highlighting the recent exploration of fluorescence lifetime imaging microscopy (FLIM) in material (molecular self-assembly, polymers, nanomaterials, and metal-organic frameworks) science research. Some of the images of the figure were adapted with copyright permission from ref. no. 74, 81, 83, 107, 108, 139, 148, 152 (Copyright American Chemical Society), ref. no. 109 (Copyright Elsevier), and ref. no. 94 (Copyright Springer).

photobleaching and low resolution are the bottlenecks of CLSM (Table 1).[54]

Considering the facts, recently, fluorescence lifetime imaging microscopy (FLIM) has been used to explore the salient features of different fluorescent or fluorophore-tagged materials.[68-73] FLIM is used to measure the fluorescence lifetime of materials, providing information on the local environment of fluorophores (Table 1).[74-80] It is particularly useful in studying molecular interactions and environmental changes within materials. FLIM can validate the presence of specific functional groups, and dynamic processes, offering insights into the chemical and physical properties of materials.[79,80] In addition, the use of FLIM for blinking and antibunching studies aided in exploring the physical properties of nanomaterials, especially for semiconductor nanocrystals.[81-91] Thus, FLIM has been invoked as a complementary tool to decipher the unique aspects of diverse materials including nanomaterials, molecular self-assembly, polymers, and metal-organic frameworks.[74,77-79, 92-98] This perspective article will highlight the importance and need of FLIM in material research by summarizing some of the recent key articles (Figure 1). In addition to the state-of-the-art knowledge of the field, the future scope of FLIM for the in-depth understanding for the development of a range of molecular materials will also be delineated.

2. FLUORESCENCE LIFETIME IMAGING MICROSCOPY (FLIM)

FLIM is a powerful imaging method that measures how long a fluorophore stays excited before emitting light, using tools like time-correlated single-photon counting (TCSPC).[99] The simplest instrumental setup of FLIM has been shown in

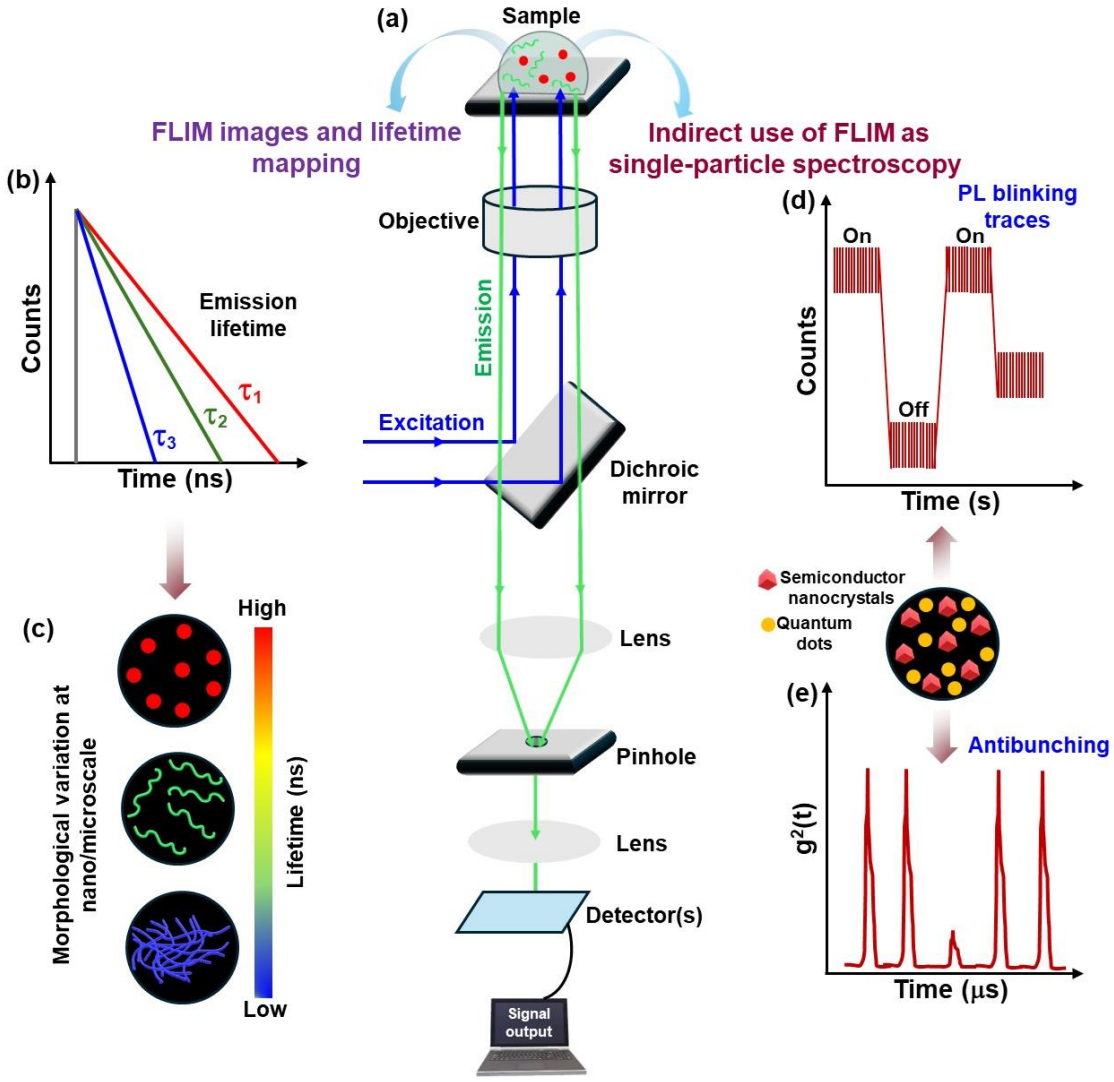

Figure 2. (a) The schematic illustration depicting the simplest instrumental setup and working principle for fluorescence lifetime imaging microscopy (FLIM). (b, c) FLIM images and lifetime mapping for the exploration of various aspects of morphological evolution in material science. (d, e) The additional use of FLIM as single-particle spectroscopy for deciphering the material aspects of semiconductor nanocrystals and quantum dots through photoluminescence blinking and antibunching analyses.

Figure 2a. The fundamental principles of FLIM, along with its instrumentation and recent advancements, have been extensively covered in the literature. Readers seeking more in-depth information are encouraged to look up earlier works, including comprehensive review articles.[70,72,79,95,100-102] A comparative analysis of salient features of FLIM with other imaging techniques like FESEM, TEM, AFM, and CLSM has been provided in Table 1.

Fluorescence lifetime is not affected by the concentration of the fluorophore, unlike intensity measurements (Figure 2b). By integrating fluorescence lifetime measurements with spatial imaging, FLIM can provide detailed maps of the fluorescence lifetimes across a sample, revealing spatial variations in the local environment such as pH, ion concentration, viscosity, and the presence of other molecules or quenchers in the proximity of the fluorophore (Figure 2c).[79] Consequently, FLIM has been extensively explored in biological and medical research to study cellular processes, protein-protein interactions, and enzyme activities.[70,80] Additionally, it is also used in clinical diagnostics, particularly in cancer research, where changes in fluorescence lifetime can indicate malignant transformations or other pathological conditions.[103-106] Apart from biological applications, recently, FLIM has also been invoked to get insights into the structural, compositional, and dynamic characteristics of various materials.[79,93,107-109]

FLIM can detect the changes in fluorescence lifetime caused by polymer cross-linking or network formation, providing insights into the final properties of polymeric

materials.[93,110,111] Shifts in fluorescence lifetime and variations in lifetime histograms are used to track changes in polymers under different environmental conditions.[110] Similarly, changes in fluorescence lifetime can reveal the aggregation state of molecular self-assembled systems, offering valuable information about their stability and functionality.[79] FLIM is also utilized to examine the crystallinity and presence of defects in materials, which have a direct impact on their optical, electrical, and mechanical properties.[74,107] Moreover, FLIM plays a significant role in studying energy transfer processes within materials, such as interactions between components in composites or within multichromophoric systems.[94] Additionally, it serves as a valuable tool for evaluating the photostability of materials by monitoring fluorescence lifetime changes during prolonged illumination.[112-114]

With the addition of all the applications discussed in the previous paragraph, FLIM has also been explored to examine the photoluminescence (PL) blinking and photon antibunching phenomena, which are critical in understanding the behavior of a single photon emitter (Figure 2d, e).[82,83,115,116] This is essential for analyzing blinking kinetics which relies on fluorescence lifetime revealing the transitions between emissive (ON) and non-emissive (OFF) states. This helps to track the blinking dynamics and quantify the "ON" and "OFF" times with high temporal resolution.[81,117,118] Additionally, FLIM provides insight into the quantum nature of fluorescence emission using photon antibunching analysis, where a single fluorophore emits photons one at a time, rather than in pairs or bursts.[83] Through TCSPC, FLIM can measure lifetime, capturing the single-photon statistics which is necessary to confirm antibunching behavior.[83] This makes FLIM invaluable in quantum optics and single-molecule studies, where an understanding of photon emission dynamics is crucial. The current road map represented in Figure 1 shows the material research that has greatly benefitted using FLIM.[74,81,83,94,107-109,139,148,152] In the next section, we will shed light on the work of various material research groups that have utilized FLIM to gain insights into the properties and dynamics of materials with a few of the recent interesting studies.

3. SEMICONDUCTOR NANOCRYSTALS

FLIM has emerged as a unique analytical tool for studying semiconductor nanocrystals, especially for understanding their optical properties at the nanoscale.[81,82] Semiconductor nanocrystals exhibit unique photophysical behaviors such as PL blinking and photon antibunching, which are essential for applications in optoelectronics and quantum computing.[83,119] FLIM enables researchers to capture the fluorescence decay times of individual nanocrystals, providing insights into the dynamics of electron-hole recombination.[116,119] By mapping fluorescence lifetimes across a sample, FLIM effectively analyzes variations in photoluminescence (PL), helping to identify blinking events where nanocrystals switch between emissive and non-emissive states.[85,115] Additionally, FLIM's ability to differentiate between fluorescence lifetimes makes it an ideal technique for studying photon antibunching, which detects and characterizes single-photon emission events.[83,120] This capability is vital for developing single-photon sources and advanced quantum communication systems, underscoring FLIM's importance in advancing semiconductor nanocrystal research. The technique has been successfully optimized to analyze fluorescent nanocrystals at the single-particle level.

3.1. PEROVSKITE NANOCRYSTALS (PNCs):

Perovskite nanocrystals (PNCs) have emerged as a crucial candidate in the development of photovoltaic and optoelectronic devices due to the presence of multiple pathways for exciton relaxation. FLIM has proven effective in understanding exciton dynamics at the single-particle level.[82,115,121-124] It has been used to study PNC kinetics based on photoluminescence (PL) blinking traces.[81,119,125-127] Depending on intensity fluctuation patterns, single nanocrystals exhibit either PL blinking, characterized by rapid transitions between high-intensity ON and low-intensity OFF states, or PL flickering, where the ON and OFF states transition occurs through a continuous intensity distribution.[125,128] The synthesis method of PNCs significantly impacts exciton dynamics and intensity fluctuations. In a recent study, 30% of as-synthesized $CsPbBr_3$ PNCs showed blinking when prepared at room temperature via antisolvent precipitation.[125] In contrast, a different intensity pattern emerged

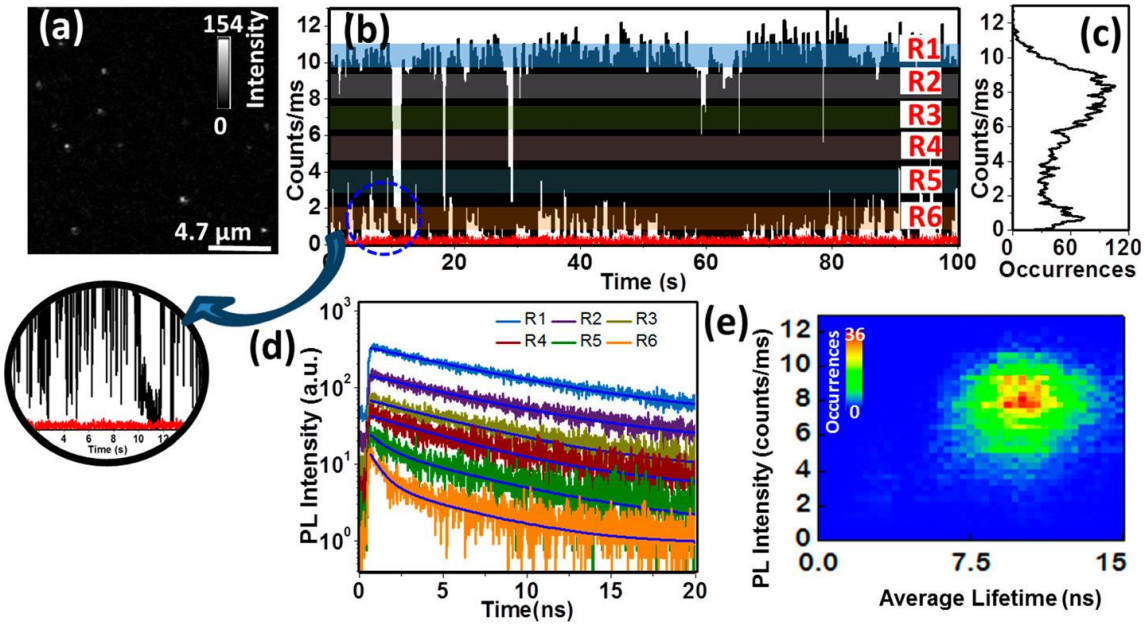

Figure 3. (a) Confocal microscope-based photoluminescence (PL) intensity image of a *CsPbBr₃* perovskite nanocrystal (PNC). (b) Time trace of the PL intensity (binning time was used 10 ms) for a single NC. The zoomed portion highlights the low-intensity "gray" states, which are nearly indistinguishable from the background (red line) or the "off" state. (c) Distribution of the observed PL intensities, (d) R1 to R6 are the PL decay profiles in which R1 - R4 are single exponential decay, R5 and R6 are biexponential decay. (e) Fluorescence lifetime intensity distribution (FLID) of a single *CsPbBr₃* NC with a false-color representation. The figure was adapted with copyright permission from ref. no. 81. Copyright American Chemical Society.

when $CsPbBr_3$ PNCs were synthesized using the hot-injection method. After analyzing 55 single NCs, 70% exhibited blinking, showing an occurrence versus intensity pattern. The PL intensity distribution revealed three distinct states: a high-intensity ON state, a low-intensity gray state, and a near-zero intensity OFF state.[81]

Ahmad *et al*. used a picomolar solution of *CsPbBr₃* PNCs which was drop-casted and dried under vacuum to study the PL blinking at the single particle level. The PL image was taken using a confocal microscope (Figure 3a). To further investigate the intensity states, the PL intensity was categorized into six levels (R1 to R6), and decay profiles were analyzed (Figure 3b).[81] The higher intensity levels (R1 to R4) exhibited single-exponential decay, while the lower intensity levels (R5 and R6) showed biexponential decay (Figure 3d). The zoomed-in portion highlights the low-intensity "gray" states, which are nearly indistinguishable from the background (red line) or the "off" state (Figure 3b). The intensity distribution of the blinking pattern for the high intensity is also reflected in the occurrences *vs*. count graph (Figure 3c). The highest intensity corresponded to an excitonic emission lifetime of approximately 8.2 ns, with lifetimes decreasing as PL intensity diminished. The intensity-lifetime scaling factor (η) for the top four intensity levels was as follows. The higher intensity levels (R1 to R4) exhibited single-exponential decay, while the lower intensity levels (R5 and R6) showed biexponential decay (Figure 3d). The zoomed-in portion highlights the low-intensity "gray" states, which are nearly indistinguishable from the background (red line) or the "off" state (Figure 3b). The intensity-lifetime scaling factor (η) for the top four intensity levels was as follows:[81,82]

$$\eta = k_{R1}:k_{R2}:k_{R3}:k_{R4} = \frac{I_1}{\tau_1}:\frac{I_2}{\tau_2}:\frac{I_3}{\tau_3}:\frac{I_4}{\tau_4} = 1.1:1.0:0.92:0.75 \quad (1)$$

The near-unity radiative recombination rates across the higher intensity levels suggest a fixed radiative rate competing with variable nonradiative rates within the NCs. The measurements that have been conducted on isolated single NCs confirm that each luminescent particle consists of a single NC rather than clusters, as suggested by the lack of biexponential decay in the R1 level (Figure 3d). One might argue that multistate emissions could originate from clusters rather than individual NCs. If each particle were a cluster of two NCs with different PL lifetimes, the decay curve for the R1 level would show a biexponential profile, which it does not. Alternatively, if the two NCs had identical

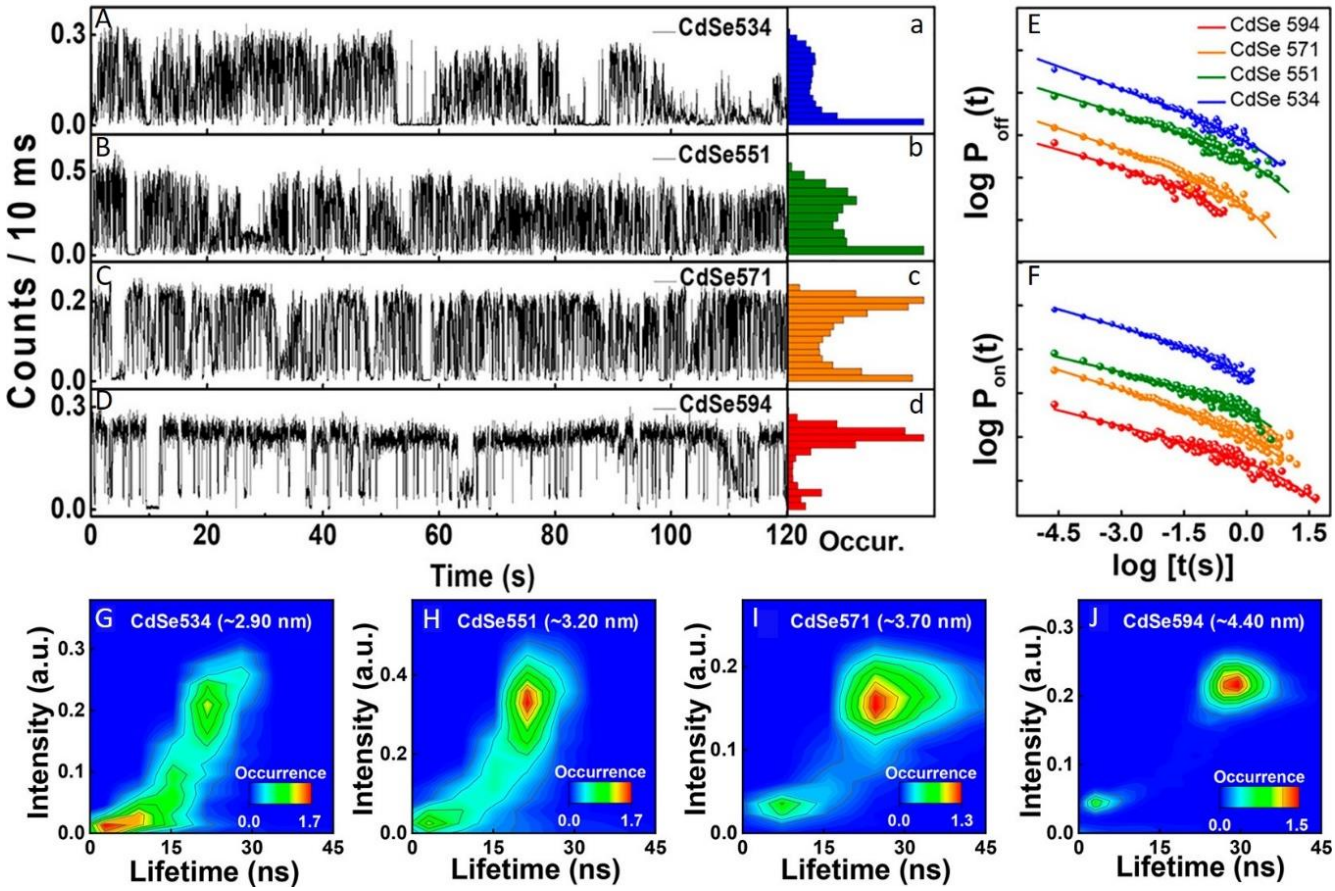

Figure 4. (A-D) Photoluminescence trajectories of (A) CdSe534, (B) CdSe551, (C) CdSe571, and (D) CdSe594 single quantum dots (QDs) having different CdSe core sizes. (a-d, middle column) Photoluminescence intensity histogram corresponding to core-shell QD. (E, F) Probability density distributions (PDDs) for the (E) OFF- (E) and (F) ON-time are shown, with the following color codes: (blue) CdSe534, (green) CdSe551, (orange) CdSe571, and (red) CdSe594. Experimental trajectories were recorded for approximately 100 QDs, and a threshold was set to distinguish between ON- and OFF-state intensities. (G-J) Fluorescence lifetime intensity distribution (FLID) plots for (G) CdSe534, (H) CdSe551, (I) CdSe571, and (J) CdSe594 are also shown. The intensity-time traces and lifetime fluctuations were obtained using a pulsed laser with 405 nm excitation with a 5 MHz repetition rate. A T3 mode based on a time-tagged time-resolved operating system has been used. The intensity time trace has been recorded for 120 seconds for each isolated QD with a bin time of 10 ms. The figure was adapted with copyright permission from ref. no. 83. Copyright American Chemical Society.

lifetimes, the PL intensity would be twice with the same lifetime, leading to an η value greater than 1.0, which is also not observed. Therefore, it is evident that each luminescent particle consists of a single NC.

The η value deviation from unity at level R4 indicates the involvement of additional processes that compete with radiative recombination. For these lower intensity levels, a lifetime component (~1 ns) becomes prominent, likely due to trion recombination, as Auger recombination also contributes to each NC blinking. Despite this, no clear patterns were observed for the 1 ns component in the fluorescence lifetime-intensity distribution (FLID) due to the low occurrence of the "gray" state population (Figure 3e). Similarly, FLIM has been used by various groups to analyze intensity fluctuations based on PL lifetime distributions.[81,82,117,119,125-127,129]

Garai *et al*. demonstrated changes in PL blinking intensity patterns using FLIM to study single cubes and nanorods of $CsPbBr_3$ PNCs. It has been observed that the ON state intensity occurrence and lifetime increased as nanorods elongated.[130] Bera *et al.* studied crack platelets, passivated crack platelets, and square platelets, and found that only the square platelets were single-photon emitters.[116] Singha *et al.* used FLIM to study the exciton dynamics of immobilized $FAPbBr_3$ PNCs and examined the effects of energy and fluence in the excited state.[82]

3.2. QUANTUM DOTS (QDs):

FLIM has played an important role in understanding the kinetics of semiconductor quantum dots (QDs) at the single-particle level as

well.[83-85,120,129,131-133] Vishnu *et al.* have extensively studied semiconductor QDs to explore the exciton dynamics and PL blinking.[83,120,131] CdSe/CdS/ZnS core/shell/shell systems with varying core sizes have been investigated to understand the exciton dynamics. The core size has been varied from 2.9 nm to 4.4 nm while keeping the shell thickness constant (Figure 4).[83] Intensity fluctuations were recorded for up to 120 seconds for different size QDs (Figure 4A-D), and it was observed that the occurrence of high-intensity (ON-state) events increased for CdSe594 (Figure 4D) which is also reflected in the occurrence *vs*. count plots (Figure 4a-d). The power law model which is based on probability density distribution (PDD) is popular to explain the blinking behavior for QDs. The combination of power law and truncated power law is used to fit the ON- and OFF-events. The PL trajectories of individual quantum dots (QDs) were recorded for 120 seconds, enabling the construction of probability density distributions (PDDs) for ON- and OFF-events (Figure 4E, F). These PDDs exhibit an initial power-law behavior transitioning into an exponential decay at longer times, consistent with a truncated power-law model (equations 2 and 3). The truncation point signifies the shift between distinct blinking, highlighting a transition from fast to slower blinking processes.

The PDDs can be fitted using the truncated power-law (TPL) function, $P_{ON}(t)$ for the ON-state and $P_{OFF}(t)$ for the OFF-state:[83]

$$P_{ON}(t) \propto t_{ON}^{-m_{ON}} exp^{-(t_{ON}/\tau_c^{ON})} \quad (2)$$

$$P_{OFF}(t) \propto t_{OFF}^{-m_{ON}} exp^{-(t_{OFF}/\tau_c^{OFF})} \quad (3)$$

The parameters 'm' and 'τ_c' represent the power-law exponent and the truncation time, respectively, with the superscripts *ON* and *OFF* indicating the corresponding ON- and OFF-events. These functions characterize a blinking process, where the behavior is described by a power-law distribution at shorter times and an exponential decay at longer times.

The exponential truncation observed in the ON-time PDD reflects an ON-to-OFF transition process characterized by a single rate constant (Figure 4E), while the OFF-time PDD represents the OFF-to-ON transition mechanism (Figure 4F). In PDD analysis, the truncation times, τ_c^{ON}(ON-to-OFF transition time) and τ_c^{OFF} (OFF-to-ON transition time), provide valuable information about the kinetics of charge trapping and detrapping. Specifically, the charge trapping rate constant (k_t) is determined as the inverse of τ_c^{ON} and the detrapping rate constant (k_d) is calculated as the inverse of τ_c^{OFF}. The ratio of τ_c^{ON} to τ_c^{OFF} corresponds to the ratio k_d/k_t, offering insight into the balance between these processes. Additionally, the power-law exponents associated with ON- and OFF-events reveal trends across the four QD sets, shedding light on the underlying blinking dynamics. The trapping probability is calculated using the following equation:

$$P_{trapping} = \tau_c^{ON}/(\tau_c^{ON} + \tau_c^{OFF}) = k_t/(k_t + k_d) \quad (4)$$

Table 2. Changes in trapping probability and ON/OFF-truncation time with varying the core size of CdSe in CdSe/CdS/ZnS core/shell/shell system.[83]

QDs	Core diameter (nm)	ON-truncation time (τ_c^{ON})	OFF-truncation time (τ_c^{OFF})	$P_{trapping}$
CdSe534	2.9 ± 0.3	0.31 ± 0.1	0.89 ± 0.4	0.73 ± 0.1
CdSe551	3.2 ± 0.1	0.45 ± 0.2	0.66 ± 0.2	0.61 ± 0.1
CdSe571	3.7 ± 0.2	0.68 ± 0.3	0.54 ± 0.2	0.49 ± 0.1
CdSe594	4.4 ± 0.2	0.93 ± 0.4	0.38 ± 0.1	0.31 ± 0.1

As the core diameter increases from 2.9 nm to 4.4 nm, the ON-truncation time increases from 0.31 to 0.93, and the OFF-truncation time decreases from 0.89 to 0.38, correlating with higher intensity PL blinking (Table 2). In smaller QDs, possibility of trapping which leads to the formation of the multiexciton generation as the wave function for electron and hole penetrates the interface of the core-shell. Photoionization from multiexciton generation accelerates Auger ionization, forming trions and enhancing fast nonradiative processes. For larger QDs, the exciton wave function is confined within the core, resulting in higher intensity and longer lifetimes due to neutral exciton recombination.[83]

3.3. FLUORESCENCE LIFETIME INTENSITY DISTRIBUTION (FLID) FOR SEMICONDUCTOR NANOCRYSTALS:

FLIM is useful to correlate the fluorescence lifetime with the intensity, captured through fluorescence lifetime intensity distribution

(FLID). FLID is particularly useful for identifying and confirming the presence of multiple fluorophores in a system. By mapping lifetime variations and intensities, it enables a deeper understanding of molecular environments and dynamics in complex systems.[81-83,118,119,125-127] Vishnu *et al.* also used FLID to analyze the CdSe/CdS/ZnS core/shell/shell system and observe multiple recombination pathways with varying core sizes (from 2.9 nm to 4.4 nm) while maintaining the same shell thickness across all four QDs (Figure 4G-I).[83] Two components were observed in the FLID plots: a component with high intensity and a longer lifetime, was assigned to neutral exciton recombination, and the second component with low intensity and a shorter lifetime was assigned to Auger recombination and trap states. The decreasing curvature of the FLID plot with increasing core diameter indicates less involvement of the Auger process, which relates to the trapping/detrapping rates and ON/OFF truncation times (as discussed earlier). Ahmad *et al.* also used FLID to study two simultaneously occurring recombination processes, but the low intensity and shorter lifetime were unclear due to the low occurrence of the gray state in *CsPbBr₃* PNCs (Figure 3e).[81]

3.4. PHOTON ANTIBUNCHING FOR SEMICONDUCTOR NANOCRYSTALS:

FLIM is also an effective technique for confirming whether a particle is a single emitter through photon antibunching experiments.[82,83,116,131,132] Photon coincidence can be analyzed using second-order photon correlation analysis:

$$g^{(2)}(t) = \frac{\langle I_1(t) I_2(t+\tau) \rangle}{\langle I_1(t) \rangle \langle I_2(t+\tau) \rangle} \quad (5)$$

The terms $I_1(t)$ and $I_2(t+\tau)$ represents the emission intensity at time t in detector 1 and after the time delay τ at detector 2, respectively. The $g^{(2)}(t)$ is a powerful analysis method to demonstrate photon antibunching. A value of $g^{(2)}(0)$ approaching zero confirms that a single photon emitter QD is being studied. This function measures the joint probability of detecting a photon at two detectors at a time $t = 0$ and at $t > 0$. For a single emitter, after emitting a photon at $t = 0$, the molecule relaxes to the ground state and cannot emit another photon until re-excited, leading to a zero probability of photon emission at $t = 0$. Vishu *et al.* took the FLIM images for CdSe/CdS/ZnS QDs with varying core sizes (Figure 5a-d). The dip in the correlation curves observed for the QDs signifies the photon antibunching (Figure 5e-f). The second-order photon correlation for CdSe/CdS/ZnS quantum dots displayed a peak with a lower magnitude at $t = 0$ compared to the side peaks.[83]

The same group used the photon antibunching technique for *CsPbBr₃* PNCs to demonstrate how facets affect multiexciton generation. They found that the enhancement of biexciton formation increases with the number of facets, from 6 (cubic) to 26 (rhombicubocatahedron), as it enhances surface polarity.[134] A similar method was employed by Singha *et al.* for $FAPbBr_3$ PNCs to confirm single-emitter behavior.[82] Thomas *et al.* also confirmed a dip in the $g^{(2)}(0)$ value approaching zero at zero time delay for the CdSe/CdS core-anisotropic shell system, confirming that the

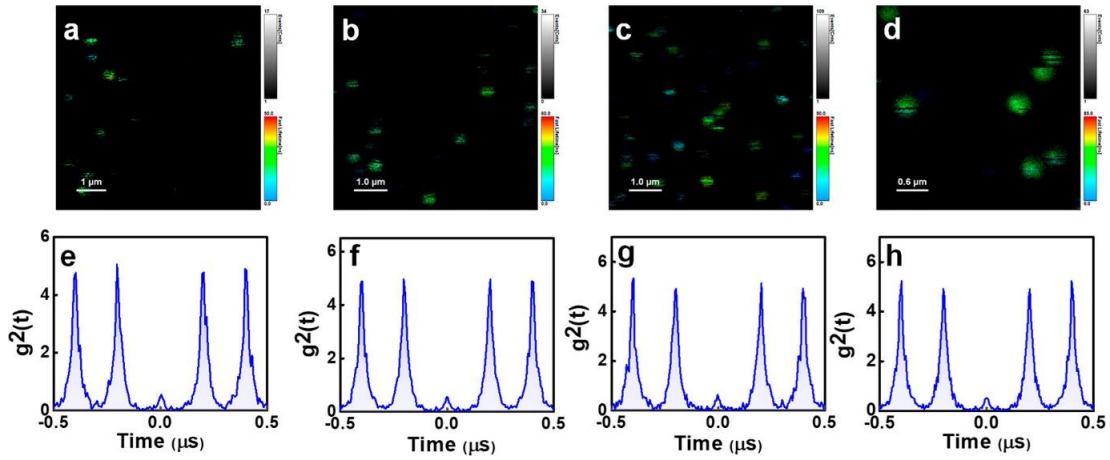

Figure 5. (a-d) FLIM images of (a) CdSe534, (b) CdSe551, (c) CdSe571, and (d) CdSe59 core-shell QDs. The second-order photon correlation (antibunching) plots of (e) CdSe534, (f) CdSe551, (g) CdSe571, and (h) CdSe594 core-shell QDs. A 405 nm pulsed laser was used to excite the samples with a repetition rate of 5 MHz. The figure was adapted with copyright permission from ref. no. 83. Copyright American Chemical Society.

exciton is localized within the core.[132] A similar dip in the $g^{(2)}(0)$ value was observed for the CdSe-CdS system with tadpole morphology, where the electron delocalizes between the CdSe core and the CdS shell, while the hole remains localized in the CdSe core. This confirms that the system is a single emitter, even though the exciton wave function is not entirely confined within the core.[131]

Thus, FLIM has proven to be an indispensable tool for advancing the understanding of nanocrystals, particularly in elucidating their photophysical properties and exciton dynamics at the single-particle level. By offering the ability to map fluorescence lifetimes across individual nanocrystals, FLIM enables researchers to explore complex phenomena like PL blinking, photon antibunching, and multiexciton generation, which are critical for optoelectronic and quantum applications. It can distinguish between multiple emissive states and track variations in lifetime intensities providing deep insights into electron-hole recombination, charge trapping, and non-radiative processes within nanocrystals. These insights are vital for optimizing the design and synthesis of nanocrystals for use in quantum dots, perovskite nanocrystals, and other advanced materials, making FLIM a crucial tool in the development of next-generation optoelectronic devices and quantum technologies.

4. MOLECULAR SELF-ASSEMBLY

FLIM has been explored as a powerful tool for studying *in situ* supramolecular aggregation processes.[45,79] It provides detailed information about the local environment and its impact on molecular self-assembly.[70,135] Fluorescence lifetime often alters due to the variations in their microenvironment, such as differences in polarity, viscosity, or the presence of quenchers.[79,113] FLIM can detect minute changes in such parameters by monitoring the fluorescence decay rates, allowing researchers to distinguish between aggregated and non-aggregated species even when their fluorescence spectra overlap. This technique is particularly useful for the visualization of the spatial distribution of self-assembled structures through lifetime maps. Furthermore, FLIM can track the dynamics of molecular aggregation providing insights into the formation, stability, and dissociation processes.[79,108,109,113,136-139]

Kundu *et al*. demonstrated the need for FLIM to decipher the spontaneous, microenvironment-sensitive dynamic molecular self-assembly process for a fluorescent alkyl-substituted dibenzophenanthroimidazole derivative, BPIB1 (Figure 6 i).[108] BPIB1 formed green emissive gel (~ 530 nm) in a binary solvent mixture of $CHCl_3$: MeOH (1 : 4, v : v). The FESEM image of BPIB1 gel showed the connected network of nanofibers (Figure 6 ii). However, the morphology could be altered due to the solvent evaporation during the drying process. To ensure morphological evolution, the *in situ* dynamic molecular self-assembly of BPIB1 was probed through FLIM (Figure 6 iii).

The FLIM images of the BPIB1 solution showed nanofiber formation (length of the fibers ~ 5 - 10 μm) at 2 min (Figure 6 iiia). Such smaller nanofibers were found to be connected to themselves to form a flower-like morphology at 4 min (Figure 6 iiib). The branching of the fibers was further becoming dense at a time point of 6 min (Figure 6 iiic). The sample at 8 min exhibited the starting of gel formation along with the other branched nano-/microstructures of BPIB1 (Figure 6 iiid). The FLIM image at 10 min showed the complete conversion of BPIB1 sol to gel (Figure 6 iiie). The CLSM images provided the same information in view of the morphological evolution of BPIB1 (Figure 6 iiif-j). However, the distinct variation in fluorescence lifetime [indicated by distinct colors in FLIM images] ascertained the influence of the microenvironment changes at different stages of the molecular self-assembly process of BPIB1 (Figure 6 iiia-e). Further, it was anticipated that the morphology of BPIB1 nano-/microstructures could be subjected to external stimuli like pH due to the presence of basic nitrogen centers. Thus, the stimuli-responsive (in the presence of acid-base *duo*) *in situ* dynamic morphological variation was probed using FLIM.[108]

The BPIB1 gel was prepared on a quartz plate and the FLIM image was captured. The connected network of nanofibers formation was noticed for native BPIB1 gel with τ_{avg} ~ 6 ns (Figure 6 iva). The broad distribution of lifetimes in the histogram profile indicated the presence of multiple heterogeneous emissive species. A

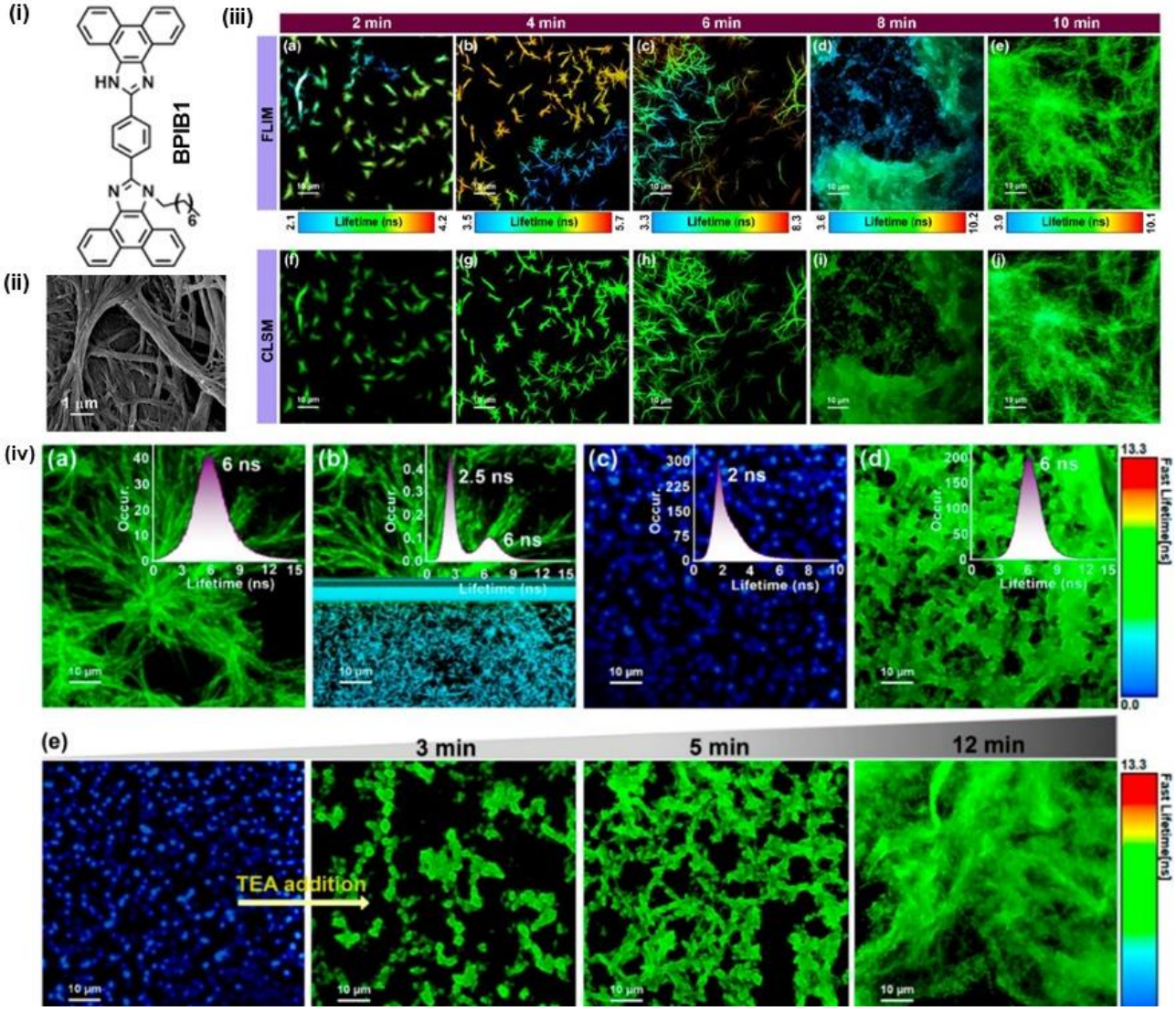

Figure 6. (i) Molecular structure of alkyl-substituted dibenzophenanthroimidazole derivative, 2-(4-(1*H*-phenanthro[9,10-*d*]imidazol-2-yl)phenyl)-1-octyl-1*H*-phenanthro[9,10-*d*]imidazole, BPIB1. (ii) Field emission scanning electron microscopy (FESEM) image of BPIB1 gel [sample preparation: the heated solution (~ 40 °C) of 1 mM of BPIB1 in 1 : 4 $CHCl_3$: MeOH (v : v) was added onto silicon wafers after the cooling and subsequently drying under vacuum]. (iii) The need for fluorescence lifetime imaging microscopy (FLIM) over confocal laser scanning microscopy (CLSM) for unraveling the time-dependent morphological evolution of molecular self-assembly of BPIB1. (a-e) The *in situ* FLIM images demonstrating the time-dependent morphological variation of BPIB1 molecular self-assembly [sample preparation for FLIM: the heated solution (~ 40 °C) of 1 mM of BPIB1 in 1 : 4 $CHCl_3$: MeOH (v : v) was added onto a quartz plate] from small nanofibers to a connected network of nanofibers to gel. The color alterations in the FLIM images ascertained the variations in fluorescence lifetime due to the microenvironmental changes during the dynamic self-assembly process. Scale = 10 μm. (f-j) CLSM images of molecular self-assembled structures of BPIB1 at different time points. Scale = 10 μm. (iv) The FLIM images deciphering the microenvironment-sensitive spontaneous reversible gel-to-sol-to-gel transformation of BPIB1. FLIM images of (a) BPIB gel, (b) trifluoroacetic acid (TFA; the demarcation in the image depicts the auto adjustment of the focus during the gel to sol transformation upon the TFA addition during the imaging)-treated BPIB1 gel, (c) nanoparticles of BPIB1 due to sol formation, and (d) reformed gel by the addition of triethylamine (TEA) to TFA-treated BPIB1 sol [Insets: the lifetime histograms highlighting the spontaneous reversible gel-to-sol-to-gel transformations; the average lifetime values for each of the distinct self-assembled states are mentioned (gel: τ_{avg} ~ 6 ns; sol: τ_{avg} ~ 2 ns)]. (e) The FLIM images of time-dependent *in situ*, spontaneous sol-to-gel formation of BPIB1 upon the addition of TEA to the TFA-treated BPIB1 sol. The figure was adapted with copyright permission from ref. no. 108. Copyright American Chemical Society.

distinct morphological transformation from the connected network of nanofibers (gel: τ_{avg} ~ 6 ns) to the smaller version of fibers (sol: τ_{avg} ~ 2.5 ns) was observed upon the addition of trifluoroacetic acid (TFA; Figure 6 ivb). Further, the histogram showed a narrow distribution of fluorescence lifetime τ_{avg} ~ 2 ns indicating the complete conversion of BPIB1 pristine gel to BPIB1 sol (Figure 6 ivc). Such conversion was found to be directed by the protonation of basic nitrogens of BPIB1 upon the TFA addition. In the next, the addition of triethylamine (TEA) to the TFA-

treated sol led to the spontaneous reformation of the gel with $\tau_{avg} \sim 6$ ns due to the deprotonation of acidified BPIB1 (Figure 6 ivd).

To probe the dynamics of the reformation of BPIB1 gel, the FLIM images were captured for 12 mins (Figure 6e). The acidified BPIB1 gel showed a complete conversion to sol with nanoparticle morphology. Then, TEA was added to the solution and FLIM images were taken at 3, 5, and 12 min. A gradual morphological transformation from connected nanoparticles (at 3 min) to a connected network of nanofibers (at 12 min) was observed due to the reformation of the gel (Figure 6e). Thus, this study paves the way for the use of FLIM as a complementary imaging tool to understand the diverse kinds of dynamic supramolecular self-assembly processes.[108] Similarly, Mañas-Torres *et al*. used FLIM to demonstrate the growth and dynamics of self-assembled fibers for short peptide chains in the presence of Ca^{2+} and Cs^{+} ions.[138] Xie *et al.* invoked FLIM to explore the nanogel formation in the presence of light stimuli for a spiropyran-based molecular system. The variation in the lifetime histograms indicated the changes in the microenvironment during the photoswitching process.[137]

Ali *et al*. investigated the aggregation process of an organic fluorophore, DDQC (7-(diethylamino)-3-(2,3-dihydrofuro[3,2-c]quinolin-4-yl)-2H-chromen-2-one), in different micellar environments to observe its aggregation behavior (Figure 7).[109] The phenomenon of aggregation-induced enhancement in emission (AIEE) was a key focus, as it indicates the potential of the system for solid-state organic emitter.[140, 141] Thus, four different types of thin films were prepared using an aqueous solution of DDQC, and DDQC in sodium dodecyl sulfate (SDS, anionic surfactant), cetyltrimethylammonium bromide (CTAB, cationic surfactant), and Triton X-100 (TX-100, neutral surfactant) micellar environments.[109]

In the next, FLIM was utilized to demonstrate the role of micellar environment on the shape of DDQC aggregates in thin films. DDQC is an example of a push-pull fluorophore where Coumarin moiety push and Quinolone moiety pull the electron density and create more electron density on quinolone nitrogen facilitating the formation of cation in the water and anionic-

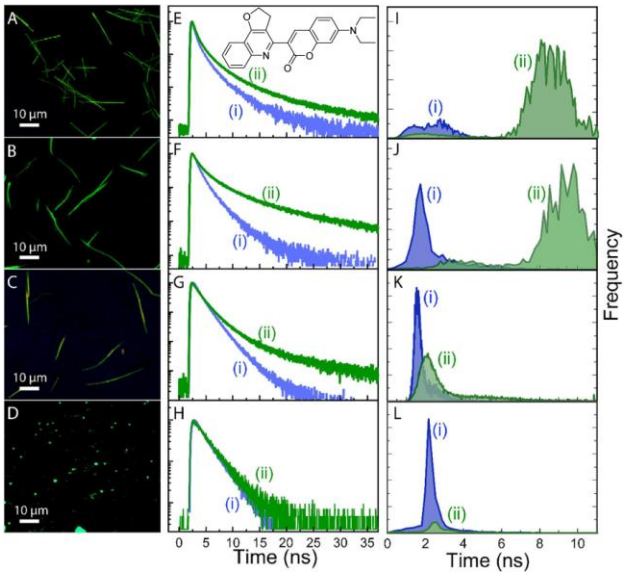

Figure 7. (A-D) FLIM images of drop-casted samples: (A) 15 µM pristine aqueous solution of DDQC (7-(diethylamino)-3-(2,3-dihydrofuro[3,2-*c*]quinolin-4-yl)–2*H*-chromen-2-one), and 15 µM DDQC in (B) 15 mM sodium dodecyl sulfate (SDS, anionic surfactant), (C) 20 mM cetyltrimethylammonium bromide (CTAB, cationic surfactant), (D) 20 mM Triton X-100 (TX-100, neutral surfactant) [Sample preparation method: the aqueous solution of DDQC was added to respective surfactant solution to achieve the desired final concentration. DDQC solution with and without surfactant was deposited on the glass slides and vacuum drying was carried out for 24 hours. In the case of TX-100 micelle, the sample was dried in an oven at 70 °C for 40 minutes]. FLIM confirmed the observation of rod-like fibers for DDQC in water, SDS, and CTAB but sphere-shape aggregation has been observed in TX-100. (E-H) Corresponding fluorescence decays where the blue decay (i) has been recorded using a bandpass filter (482 ± 17 nm) and green decay (ii) has been recorded using a long pass filter (>532 nm). (I-L) Lifetime histograms were obtained using blue bandpass [λ_{em} (i) = 482 ± 17 nm] and green long pass [λ_{em} (ii) >532 nm] filters. The figure was adapted with copyright permission from ref. no. 109. Copyright Elsevier.

charged species in SDS micelles. On the contrary, it remains neutral in the cationic charged (CTAB) and neutral (TX-100) micelles. Rod-shaped emissive aggregates are formed in films prepared of DDQC in water (Figure 7A), DDQC in SDS micelle (Figure 7B), and DDQC in CTAB micelle (Figure 7C), while spherical aggregates are predominantly observed in TX-100 micelle (Figure 7D). The variation in micellar structure may be attributed to differences in the strength of interactions between water molecules and the micelle cores, which depends on whether the micelles are ionic or nonionic.[142] The diverse morphologies of micelles have been widely reported in the context of some modifications.[109,142-144]

The fluorescence decay of the films prepared of DDQC in water using a long pass filter >532 nm (green) was slower compared to the decay recorded using a 482 nm (blue) bandpass filter (Figure 7E). The green emission primarily showed lifetimes in the 6-10 ns range, whereas the blue emission exhibited lifetimes in the 2-4 ns range (Figure 7I). Notably, the distribution of longer lifetimes displayed a higher modal frequency. In the presence of SDS, the fluorescence decay of DDQC has become more dependent on the emission wavelength compared to that in water (Figure 7F). It has been observed that the lifetime distribution slightly shifts to the longer value for the emission recorded using a long pass filter (green, Figure 7J). This observation suggests the presence of cationic species due to the presence of trace amounts of water leads to DDQC protonation in SDS micelle. Meanwhile, the blue emission, originating from micellized neutral fluorophore monomers, had a sharper lifetime distribution and maximum at 2 ns. This indicates that while the cationic form of DDQC exhibits strong aggregation-induced emission enhancement (AIEE), the micellized neutral monomers do not display a similar behavior.

In contrast, the wavelength dependence of fluorescence decay was less significant in CTAB (Figure 7G) and was absent in TX-100 (Figure 7H). For both cases, the lifetime distributions peaked around 2 ns (Figure 7K, L). These observations confirm that in TX-100, the cationic DDQC molecules have been converted to their neutral form upon water removal. This transformation is likely driven by the shift in prototropic equilibrium occurring in the wet palisade layer of TX-100 micelles. Thus, this work highlights the use of FLIM to understand molecular aggregation and kinetics in different micellar environments.[109]

Kistwal *et al*. have demonstrated the importance of FLIM for analyzing the morphological evolution and aggregation behavior of DBMPT (dimethyl-2,5-bis[4-(methoxyphenyl)amino] terephthalate) in the presence of the surfactant Tween 40 (Figure 8).[139] The cryo-TEM and FLIM images showed a gradual evolution of DBMPT nanoparticles (diameter ~ 100 nm) to nanorods (length ~ 4 µm) with varying concentrations of Tween 40 from 0

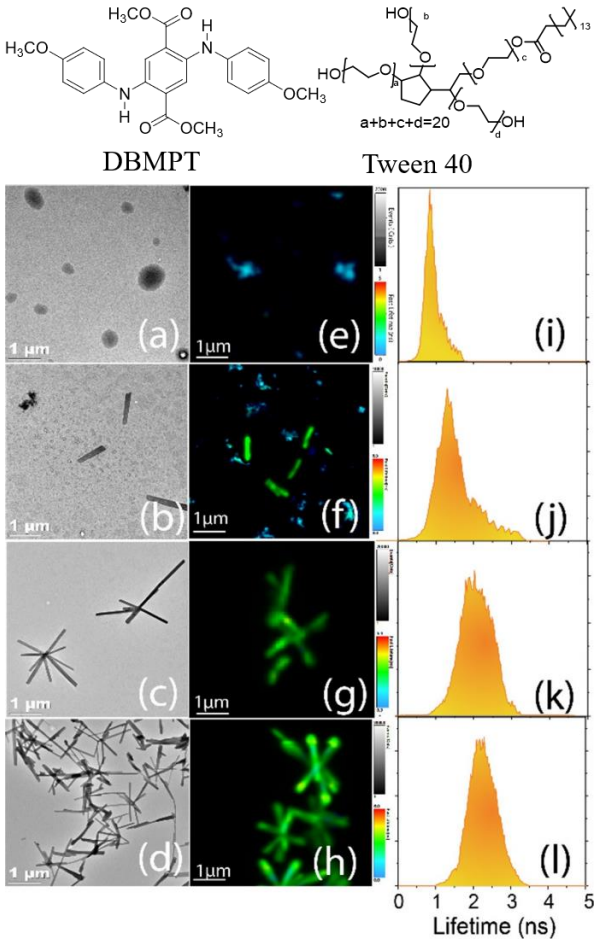

Figure 8. Top: Molecular structures of DBMPT (dimethyl-2,5-bis[4-(methoxyphenyl)amino] terephthalate) and Tween 40. (a–d) Cryo-transmission electron microscopy images, (e–h) FLIM images, and (i–l) fluorescence lifetime histograms of 50 µM DBMPT in different concentrations of Tween 40. The sample in images (a, e, i) is for 50 µM pristine DBMPT, (b, f, j) is for 50 µM DBMPT in 12 µM Tween 40, (c, g, k) is for 50 µM DBMPT in 30 µM Tween 40, and (d, h, l) is for 50 µM DBMPT in 60 µM Tween 40 (λ_{ex} for all the images = 532 nm). These panels illustrate the effect of Tween 40 concentration on the fluorescence lifetime distribution and morphology of DBMPT. The figure was adapted with copyright permission from ref. no. 139. Copyright American Chemical Society.

µM to 60 µM, respectively (Figure 8a-h). The fluorescence lifetime distribution histogram reveals that the lifetime of 1 ns is shifted from a narrow distribution for the nanoparticles in the absence of Tween 40 to a longer lifetime of 2.5 ns with a broader distribution for nanorods at the highest surfactant concentration (60 µM, Figure 8i-l). The narrow distribution of lifetime indicates the homogeneous distribution of nanoparticles, whereas the broader distribution of lifetime reflects the presence of multiple emissive species having different dimensions of nanorods. In addition, the shift in lifetime is directly associated with the transition from spherical nanoparticles to nanorods, due to the variation in molecular

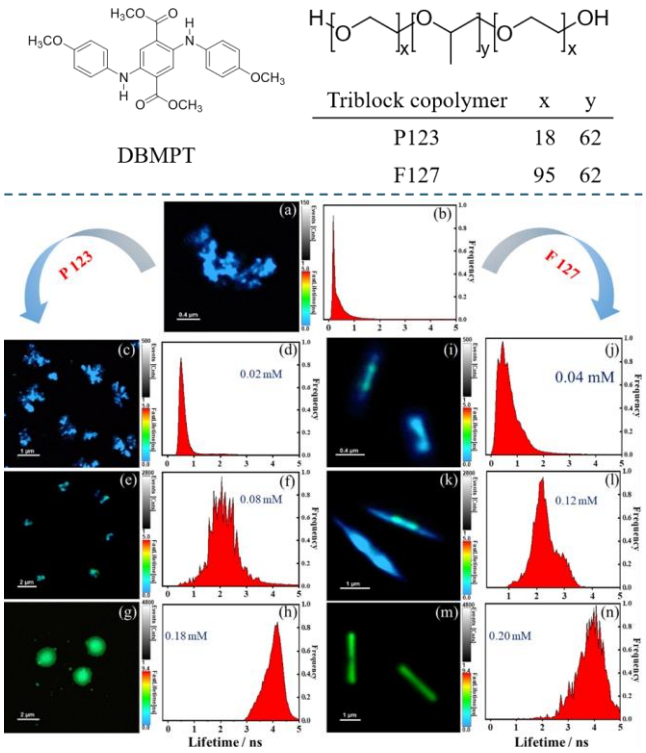

Figure 9. Lifetime-weighted fluorescence images of (a) DBMPT homoaggregates, (c, e, g) DBMPT–P123 mixed aggregates, and (i, k, m) DBMPT–F127 mixed aggregates. The corresponding fluorescence lifetime distributions are shown in panels (b), (d, f, h), and (j, l, n), respectively. The concentrations of P123 and F127 (in mM) are indicated alongside each lifetime distribution histogram. These images and histograms reveal how the aggregation environment, influenced by varying concentrations of P123 and F127, affects the fluorescence lifetime characteristics of DBMPT. This analysis provides insight into the interaction between DBMPT and the micellar structures formed by P123 and F127, showcasing the impact of micelle type and its concentration on the photophysical behavior of DBMPT. The figure was adapted with copyright permission from ref. no. 140. Copyright American Chemical Society.

packing and intermolecular interactions in the presence of Tween 40. The agreement between FLIM and cryo-TEM results confirms the formation of nanorods in solution rather than in solid state due to solvent evaporation (Figure 8). Thus, the study provides insight into the molecular dynamics and aggregation processes in a non-invasive and detailed manner.[139]

In a similar kind of study, Rakshit *et al*. demonstrated the molecular interactions of DBMPT with triblock copolymers P123 and F127 using FLIM to emphasize the formation dynamics and morphological evolution of molecular aggregates (Figure 9).[140] The temporally and spatially resolved FLIM image profiles distinctly differentiated the different morphological structures formed by DBMPT with P123 (Figure 9c, e, g) and F127 (Figure 9i, k, n). The result ascertained that after incorporation of DBMPT, the fluorescence lifetime significantly increased for the triblock copolymers leading to morphological variation of the molecular aggregates due to the impact of the microenvironment and molecular packing. As revealed from FLIM data, DBMPT exhibited spherical aggregates in an aqueous medium with an average diameter of ~ 150 ± 30 nm (Figure 9a).

The fluorescence lifetime distribution showed a sharp band ~ 0.2 ns due to the formation of homogeneous aggregates (Figure 9b). In addition, a lower intense broad lifetime distribution was noticed at ~ 4 ns. This observation certainly indicated the existence of microheterogeneity in homogeneous aggregates of DBMPT in aqueous medium. On the contrary, with the subsequent addition of P123 the lifetime distribution of DBMPT became broader indicating the presence of considerable portions of microheterogeneity in the system (Figure 9d, f, h). A similar trend was noticed in the case of F127 (Figure 9j. l. n).[140] Thus, this work highlighted the effective use of FLIM to demonstrate the transition between different morphologies. Additionally, FLIM provides vital insights into the molecular dynamics and aggregation mechanisms at a microscopic level and hence it offers a comprehensive understanding of the aggregation processes in solution.

5. POLYMER

FLIM has also evolved as an advanced tool for investigating polymers at the microscopic level. It provides insights into the local environment, molecular interactions, and dynamic processes that are not accessible through intensity-based fluorescence imaging alone.[93,145] FLIM can be used to detect the heterogeneity in the polymer matrices and solvent-polymer interactions, monitoring polymer dynamics.[110] In addition, FLIM can help in understanding photophysical processes in polymers, such as energy transfer, quenching, and photobleaching.[146,147] By mapping the fluorescence lifetime of dyes or proteins embedded in polymers, the photostability and efficiency can be visualized across the sample.[110,145,148-151] In this section, we will highlight a few exciting works in which FLIM was used to explore different aspects of the polymers.[74, 148, 152]

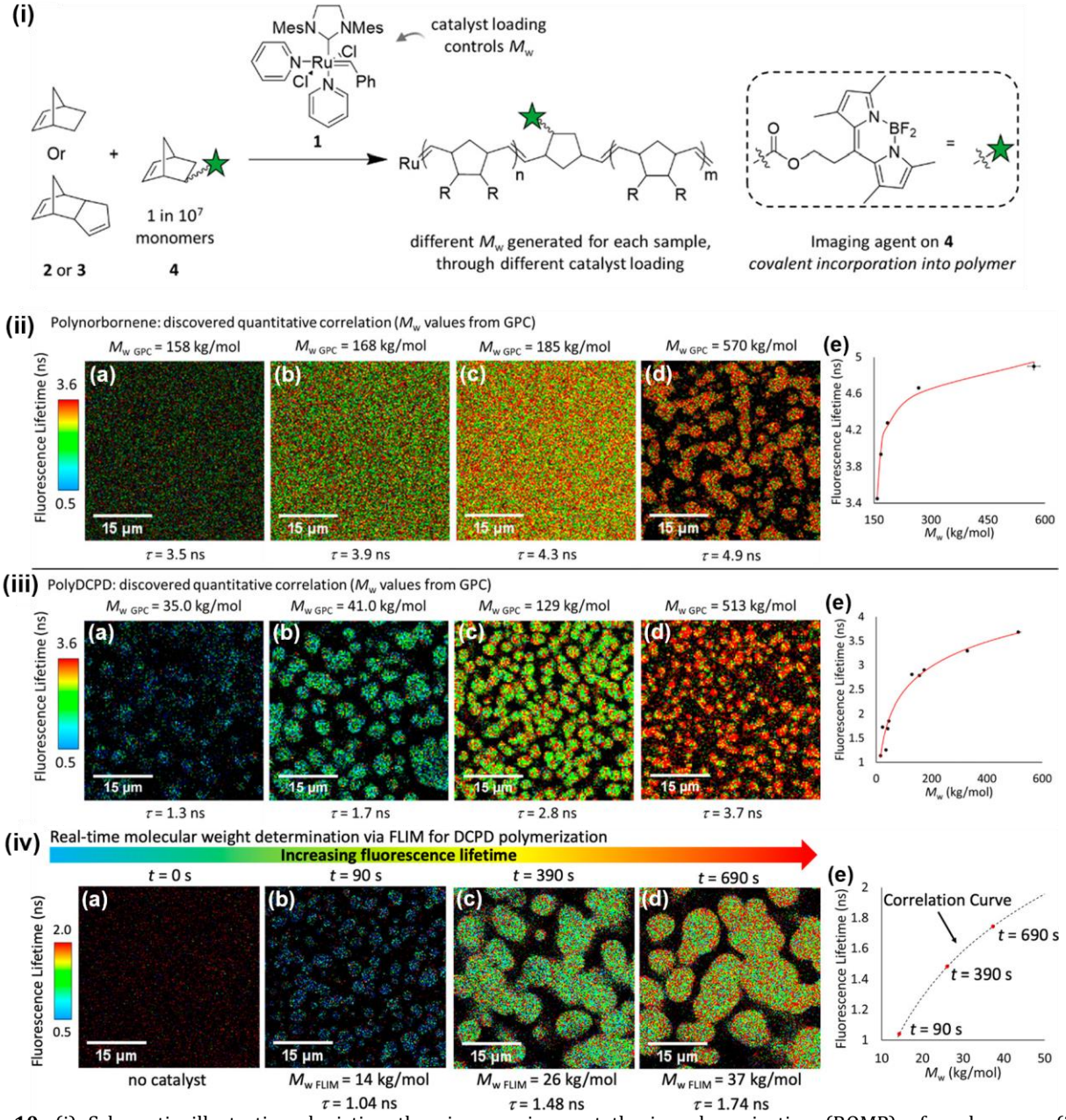

Figure 10. (i) Schematic illustration depicting the ring-opening metathesis polymerization (ROMP) of norbornene (2) or dicyclopentadiene (DCPD, 3) monomers using Grubbs third-generation catalyst (1) in the presence of low amounts of doped imaging agent 4. (ii) FLIM images of polynorbornene solution at different reaction timepoints (a-d). The average fluorescence lifetimes (τ) are obtained from lifetime histograms. The molecular weight (M_w) of polymer solutions is determined using gel permeation chromatography (GPC). FLIM images depicting the gradual increase of τ with increasing molecular weight of the polymer (a-d). (e) The correlation curve between the average fluorescence lifetime and molecular weight for the polynorbornene system (R^2 = 0.99). (iii) FLIM images of polyDCPD solution at different reaction time points (a-d). The average fluorescence lifetimes (τ) are obtained from lifetime histograms. The molecular weight (M_w) of polymer solutions is determined using gel permeation chromatography (GPC). FLIM images depicting the gradual increase of τ with increasing molecular weight of the polymer (a-d). (e) The correlation curve between the average fluorescence lifetime and molecular weight for the polyDCPD system (R^2 = 0.95). (iv) Determination of molecular weight during polymerization reaction using FLIM. All the FLIM images were taken at the same location for a one-time DCPD polymerization reaction at different time points of (a) t = 0 s (no catalyst), (b) t = 90 s, (c) t = 390 s, and (d) t = 690 s. (b) The molecular weight at different time points was calculated using the τ values obtained from the FLIM images and the correlation calibration curve in Figure iii, e. The figure was adapted with copyright permission from ref. no. 152. Copyright American Chemical Society.

Garcia *et al*. demonstrated a unique approach to determine the molecular weight (M_w) during the *in situ* polymerization reaction using FLIM (Figure 10).[152] The method is real-time, has no need for the isolation of samples, provides sub-ensemble information, and is applicable for both soluble and insoluble polymers. As a model reaction, the ring-opening metathesis polymerization (ROMP) of norbornene (2) or dicyclopentadiene (DCPD, 3) monomers using

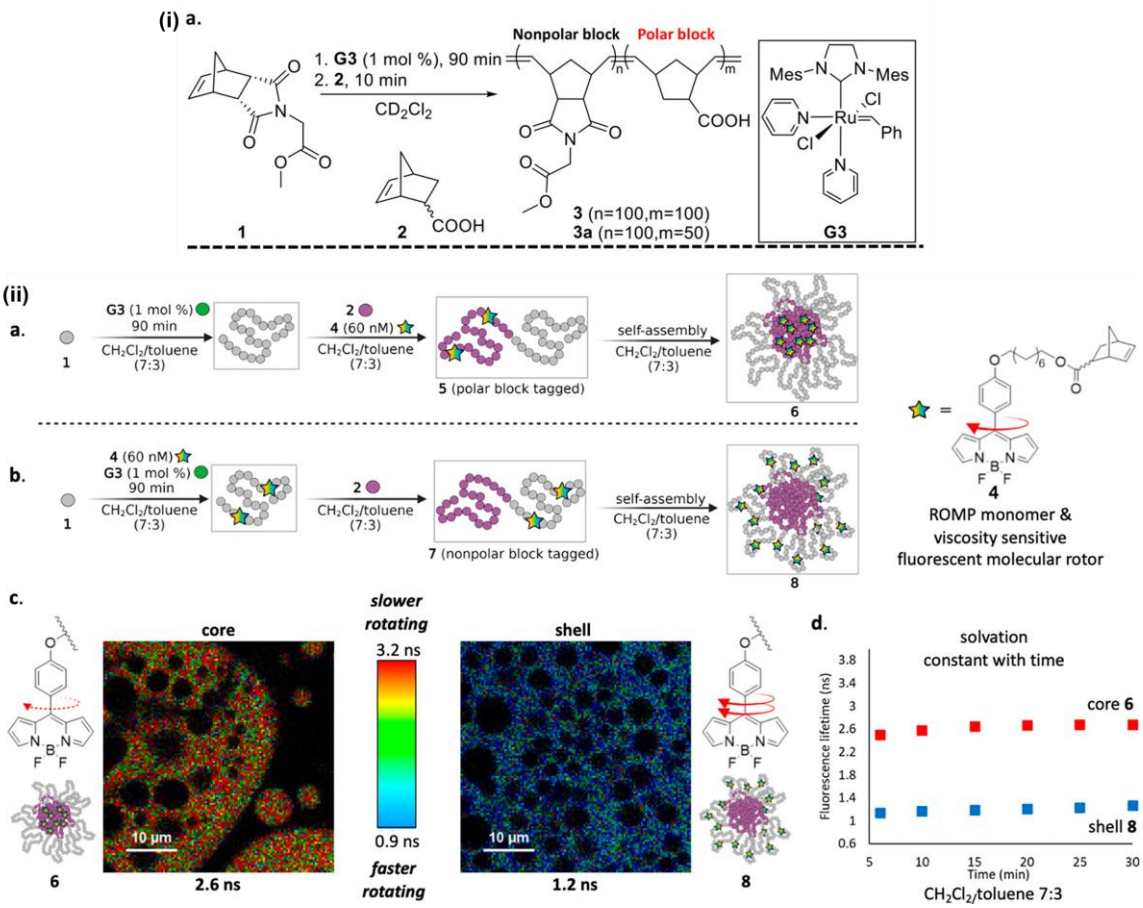

Figure 11. (i) Schematic illustration depicting the block copolymerization between monomer 1 (nonpolar system) and monomer 2 (polar system) in the presence of Grubbs third generation catalyst (G3). (ii, a) Selective tagging of the fluorescent molecular rotor (4) in monomer 2 leading to the formation of polar block tagged system 5 which self-assembled to a core-shell structure 6. (ii, b) Tagging of the fluorescent molecular rotor (4) in monomer 1 leading to the formation of nonpolar block tagged system 7 which self-assembled to a core-shell structure 8. (c) FLIM images of the core region of 6 and the shell region of 8 in 7:3 CH_2Cl_2/toluene. (d) Fluorescence lifetime *vs*. time profile for both the self-assembled structures of block copolymers 6 and 8. The figure was adapted with copyright permission from ref. no. 74. Copyright American Chemical Society.

Grubbs third-generation catalyst (1) was considered (Figure 10 i). A very low amount of imaging agent 4 was added to the reaction mixture (Figure 10 i). The molecular weight (M_w) of polymer solutions was determined using gel permeation chromatography (GPC). A sheet-like morphology was observed for polynorbornene at lower $M_{w,GPC}$ (Figure 10 iia-c). In contrast, particle-type structures were noticed for the polynorbornene with higher $M_{w,GPC}$ (Figure 10 iid). In addition, the FLIM images displayed a gradual increase in fluorescence lifetime from 3.5 ns to 4.9 ns for the enhancement of $M_{w,GPC}$ from 158 kg/mol to 570 kg/mol (Figure 10 iia-d). On the other hand, polyDCPD having different molecular weights exhibited particle-type morphology (Figure 10 iiia-c). Like polynorbornene, polyDCPD also exhibited gradual fluorescence lifetime enhancement with increasing molecular weight (Figure 10 iiia-d).

Figure 10 iie and Figure 10 iiie show the correlation curve between the average fluorescence lifetime (obtained from FLIM) and molecular weight (determined through GPC) for the polynorbornene and polyDCPD systems, respectively. Furthermore, to demonstrate the real-time determination of molecular weight solely by FLIM, a DCPD polymerization reaction was carried out (Figure 10 iv). The FLIM images were taken from the same region of the sample at different time points of 0 s (no catalyst), 90 s, 390 s, and 690 s of polymerization (Figure 10 iva-d). The average lifetime obtained at different time points from FLIM was plotted in the correlation curve of the polyDCPD system and the molecular weights ($M_{w,FLIM}$) were calculated (Figure 10 ive). Thus, this study opens a new direction for FLIM which can be further utilized for various polymeric systems.[152]

Eivgi *et al*. used FLIM as a more sensitive analytical tool as compared to that of ^{1}H NMR to

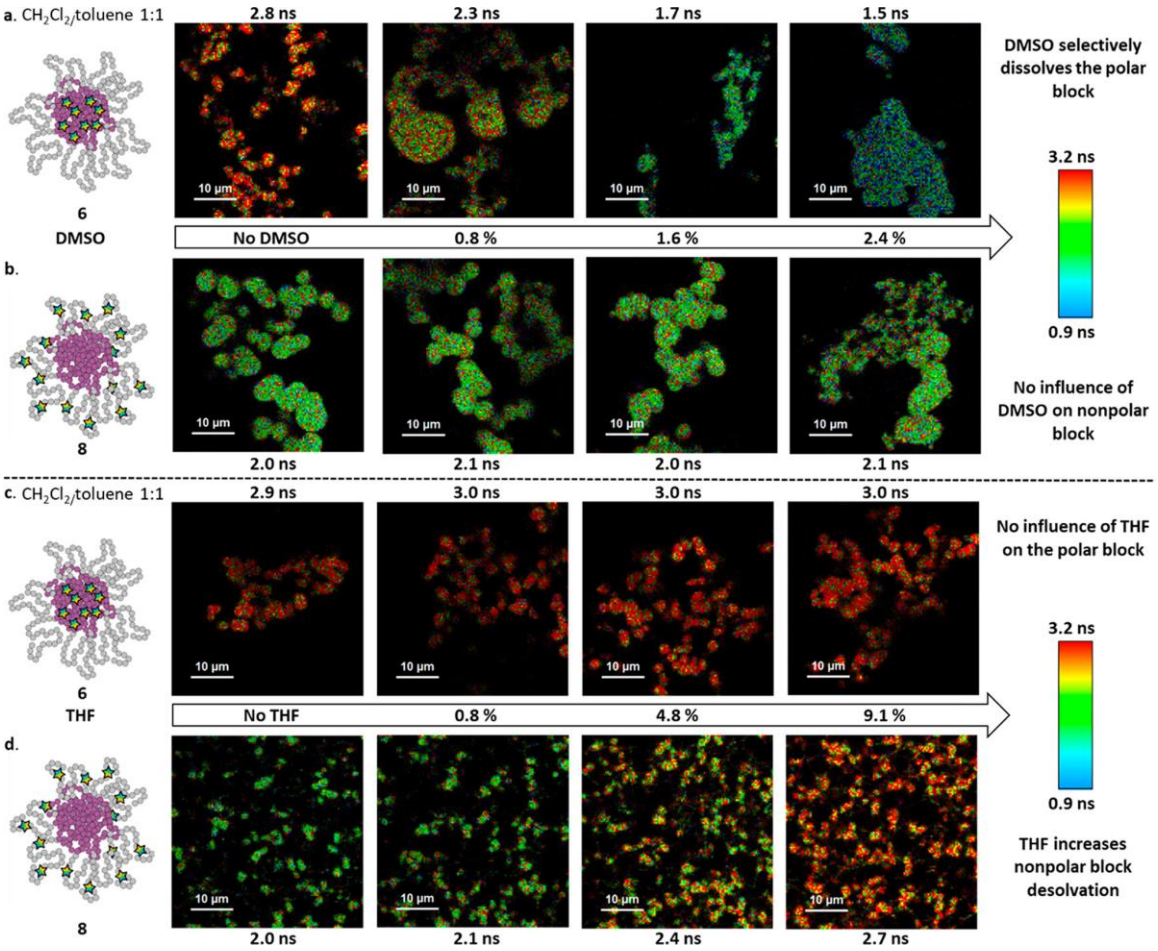

Figure 12. Probing the block-selective solvation using FLIM. FLIM images of (a) block copolymer of 6 and (b) block copolymer of 8 in CH_2Cl_2/toluene 1:1 with the gradual addition of DMSO up to 2.4%. FLIM images of (c) block copolymer of 6 and (d) block copolymer of 8 in CH_2Cl_2/toluene 1:1 with the gradual addition of THF up to 9.1%. The variation of the fluorescence lifetimes is mentioned. The increase in the fluorescence lifetime due to the addition of DMSO in 6 indicating the disassembly of the only polar blocks whereas the variation in the lifetime due to the addition of THF in 8 indicating the disassembly of the only nonpolar blocks. The figure was adapted with copyright permission from ref. no. 74. Copyright American Chemical Society.

demonstrate the solvation dynamics of an amphiphilic block copolymer system.[74] The polymerization between monomer 1 (nonpolar system) and monomer 2 (polar system) in the presence of Grubbs third generation catalyst (G3) led to the formation of amphiphilic polymers (3, 3a; Figure 11 ia). To understand the solvation of such polymers by FLIM, it is necessary to tag fluorescent molecules in either the polar or nonpolar polymeric backbone. Thus, a BODIPY-based viscosity-sensitive molecular rotor (4) was chosen (Figure 11 iia, b).

The molecular rotor was tagged with both monomers separately. In a typical procedure, 60 nM solution of 4 and monomer 2 was mixed with a living homopolymer of 1 to obtain polar copolymer 5. In CH_2Cl_2/toluene (7:3) solvent mixture, copolymer 5 formed the core-shell structure 6 (Figure 11 iia). On the other hand, molecule 4 was mixed with monomer 1 and G3 to synthesize nonpolar block tagged copolymer 7 which further showed the core-shell structure 8 in CH_2Cl_2/toluene (7:3; Figure 11 iia). The FLIM images of the block copolymer of 6 in CH_2Cl_2/toluene showed $\tau_{avg} \sim 2.6$ ns from the core (as only the core contains molecular rotor 4). On the contrary, a lower $\tau_{avg} \sim 1.2$ ns was noticed for the block copolymer of 8 under similar conditions (Figure 11 iib). The higher fluorescence lifetime of the rotor in the core is due to the more rigid environment. The no change in lifetime values for both core 6 and shell 8 over time indicated the constant solvation of the block copolymers in CH_2Cl_2/toluene (Figure 11 iic, d).[74]

Further, the solvation dynamics of both polymers were monitored in dimethyl sulfoxide (DMSO) and tetrahydrofuran (THF). The self-assembled structure of 6 in 1:1 CH_2Cl_2/toluene solvent mixture exhibited $\tau_{avg} \sim 2.8$ ns in the FLIM image. Only a 2.4% addition of DMSO in the 1:1

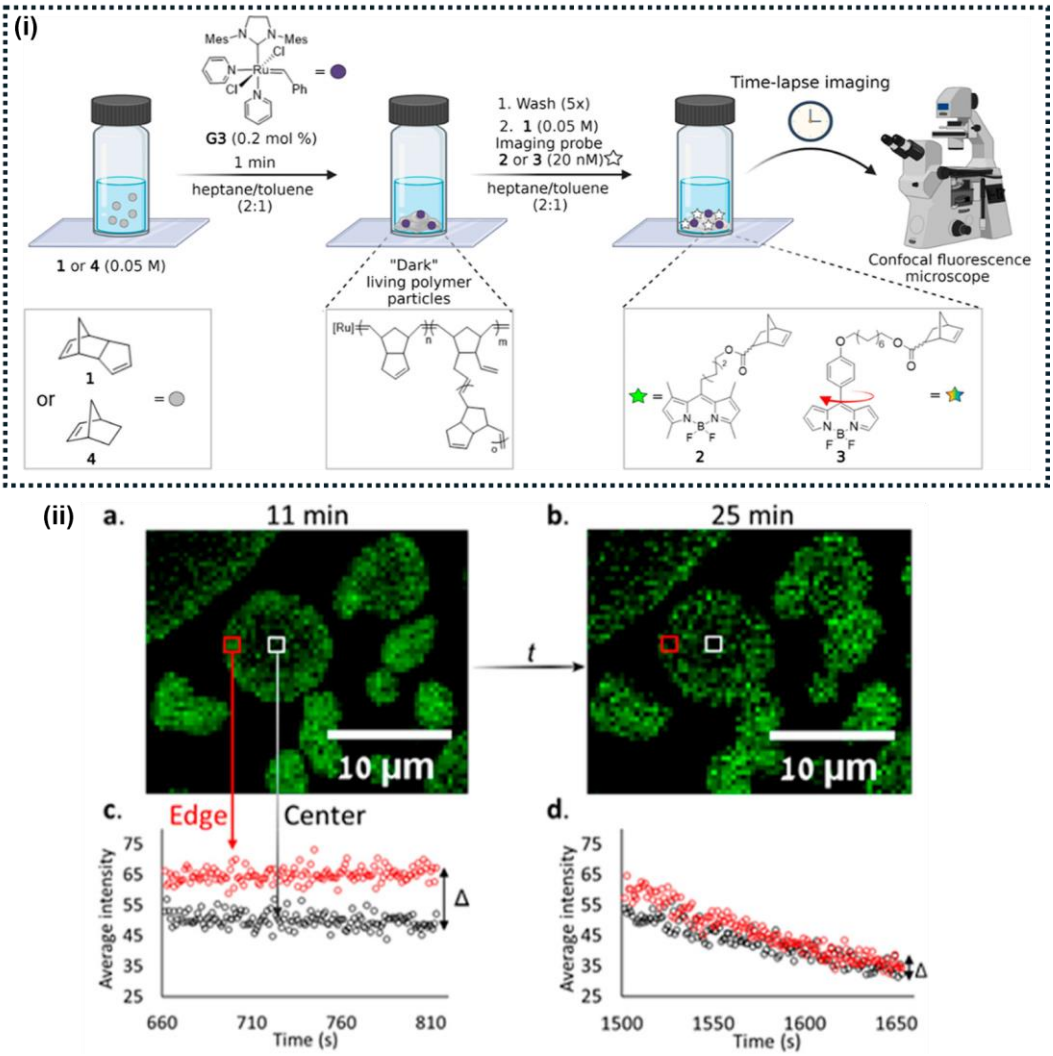

Figure 13. (i) Schematic illustration highlighting the catalytic ring opening metathesis polymerization (ROMP) reactions of the monomer 1 or 4 using Grubbs third-generation catalyst (G3). Followed by the insertion of norbornene-functionalized BODIPY imaging agents 2 or 3 into the polymeric backbone. (ii) Fluorescence intensity-based images of polydicyclopentadiene (polyDCPD) polymer particles after (a) 11 min and (b) 25 min of G3 catalyst addition. The average fluorescence intensity profiles of polyDCPD particles after (c) 11 min and (d) 25 min of catalyst addition. The black data points indicate the average fluorescence intensity at the center region of the polymer particles whereas the red data points show the average fluorescence intensity of the edge region of the polymer particles. The figure was adapted with copyright permission from ref. no. 148. Copyright American Chemical Society.

CH_2Cl_2/toluene solution of block copolymer 6 led to the decrease of fluorescence lifetime to 1.5 ns due to the disassembly of polar core structure in the presence of polar solvent DMSO (Figure 12a). However, no such variation in the fluorescence lifetime was noticed for the self-assembly of copolymer 8. The result ascertained the no influence of polar solvent like DMSO on the assembly-disassembly process of nonpolar block in 8 (Figure 12b).[74]

An opposite trend in the FLIM result was noticed in the case of THF addition to the self-assembly of block copolymers 6 and 8. No change in lifetime was observed for 6 with a gradual addition of 9.1% THF (Figure 12c). The result indicated that THF did not alter the assembly-disassembly dynamics of the polar block. Nonetheless, an increase in a lifetime from 2 ns to 2.7 ns was observed with the addition of 9.1% of THF in block copolymer 8 due to the nonpolar block dissolvation and stronger chain-chain interactions (Figure 12d). This study shows that FLIM is a useful method for understanding how block-selective solvation drives the assembly and disassembly of self-assembled amphiphilic block copolymers.[74]

Eivgi *et al*. highlighted the use of FLIM as a complementary analytical tool along with CLSM to explore the impact of microenvironment changes on the catalytic activity during the ring-opening metathesis polymerization (ROMP) reactions.[148] Dicyclopentadiene monomer (1) and

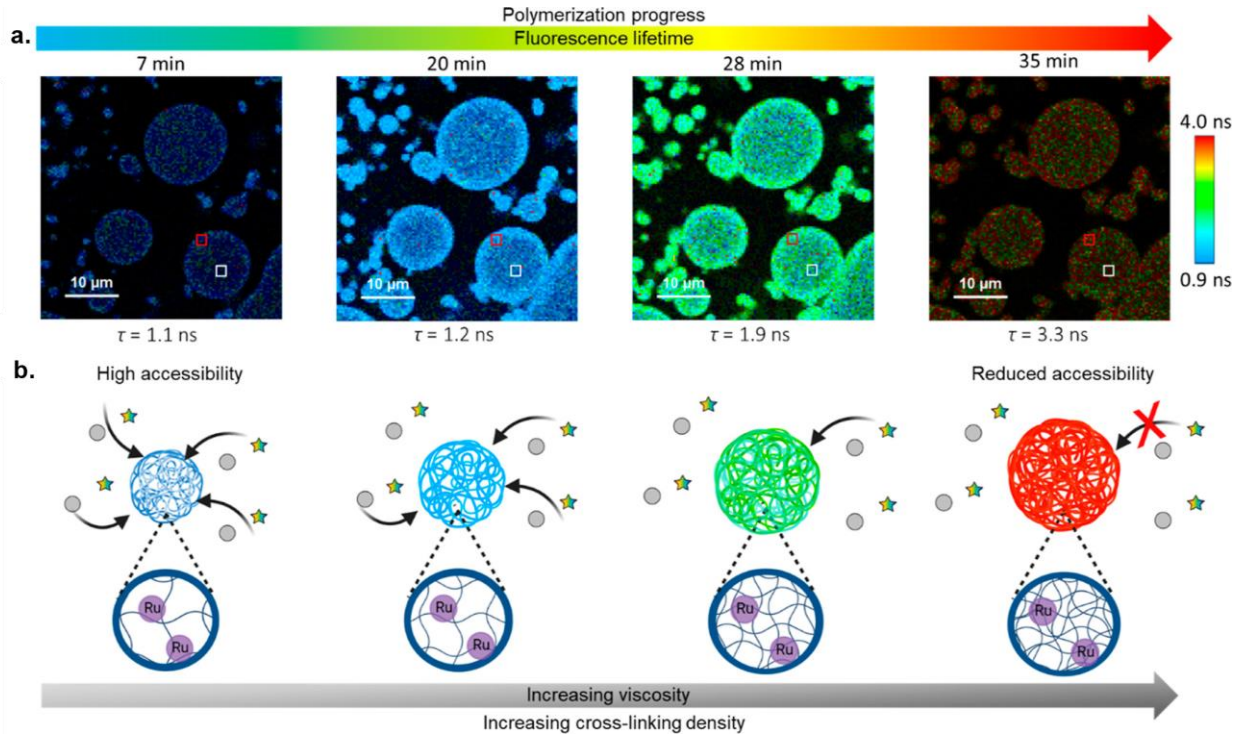

Figure 14. (a) FLIM images of DCPD polymer during the progression of the polymerization reaction over 35 min of timeframe using the molecular rotor 3. The variation of the average fluorescence lifetime (τ) of the same polymer at the same points is mentioned. (b) The plausible mechanism of microenvironment-sensitive catalytic activity during the polymerization reaction. The figure was adapted with copyright permission from ref. no. 148. Copyright American Chemical Society.

Grubbs third-generation catalyst (G3) were mixed in a heptane/toluene (2:1) solvent mixture to initiate the polymerization reaction. Once the dark (nonfluorescent) living polymer was formed then the polymer particles were washed thoroughly. To make the polymer emissive, norbornene-functionalized BODIPY [2 (for CLSM sample) or 3 (for FLIM sample); both 2 and 3 are viscosity-sensitive molecular rotors] were added to the polymers and the sample was used for imaging studies (Figure 13 i).[148]

Figure 13 iia and Figure 13 iib show the fluorescence intensity-based images of polydicyclopentadiene (polyDCPD) polymer particles decorated with the molecular rotor 2 after 11 min and 25 min of catalyst addition, respectively. At 11 min, the edge region of the polymer particle exhibited higher fluorescence intensity than the core region due to the lower accessibility of the monomer in the core (Figure 13 iic). On the contrary, after 25 min of the catalyst addition, both the edge and core regions showed almost the same catalytic activities (Figure 13 iid). It was anticipated that the catalytic activity was reduced with increasing reaction time due to the increasing polymer cross-linking which restricted the diffusional motion of the monomer.[148]

To validate the hypothesis, FLIM was used to elucidate the growth of DCPD polymer decorated with fluorescent molecular rotor 3. The FLIM images were taken from the same region of a single polymerization reaction. After 7 min of the reaction, the polymer particle showed an average fluorescence lifetime ~ 1.1 ns due to the lower local viscosity (Figure 14a). However, an enhancement in average fluorescence lifetime to ~ 3.3 ns was noticed after 35 min of the reaction time due to the diffusional restriction of molecular rotor 3 (Figure 14a). Figure 14b demonstrated the plausible mechanism of microenvironment-sensitive catalytic activity during the polymerization reaction which indicated that the diffusional restriction of the monomers towards the catalytic centers in the highly cross-linked polymer was the prime reason for the decrease in the rate of the polymerization reaction. Hence, the discussion in this section highlights the judicious use of FLIM as an emerging tool to decipher the diverse aspects of polymeric materials.[148]

6. METAL-ORGANIC FRAMEWORK (MOF)

FLIM is also explored to study the photophysical properties of MOFs. The energy transfer mechanisms and the interactions between metal nodes and organic linkers within the MOF

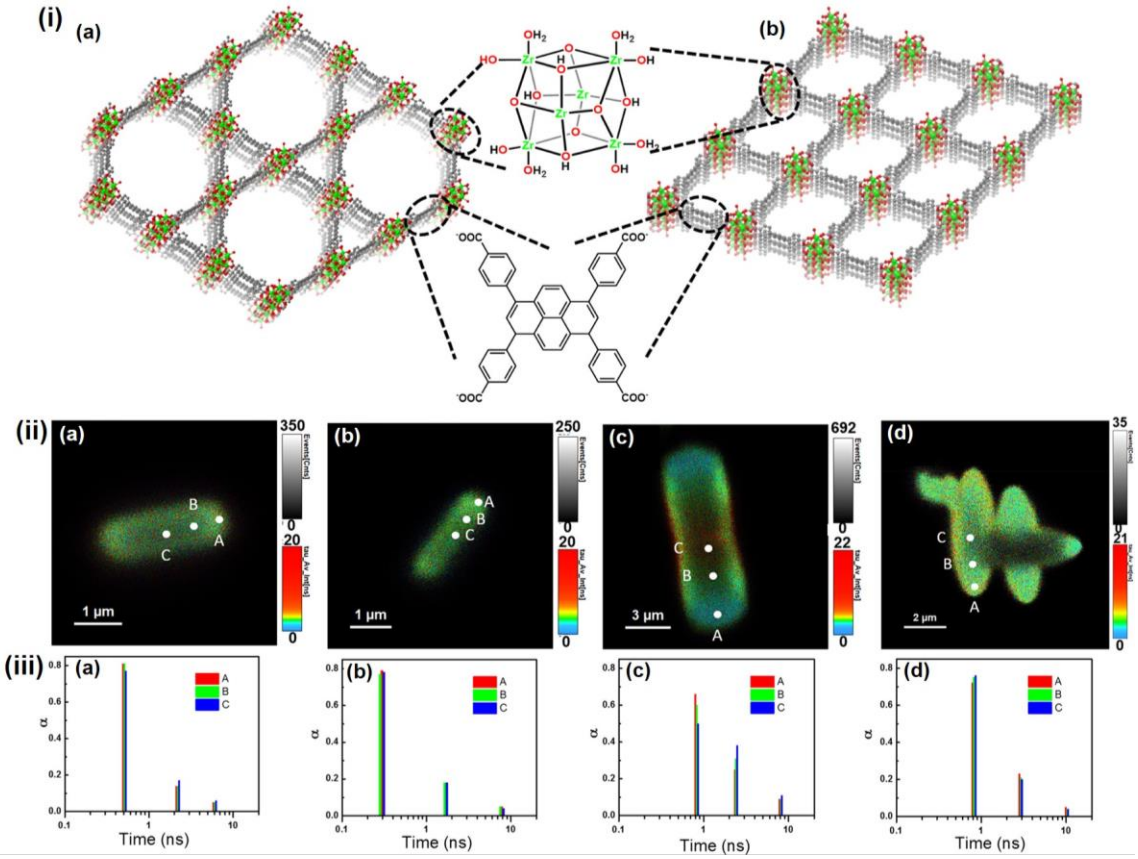

Figure 15. (i) Structure of Zr-based metal-organic framework, NU-1000. The topology of (a) NU-1000 and (b) NU-901. (ii) Fluorescence lifetime microscopy images of (a) NU-1000-1, (b) NU-1000-2, (c) NU-1000-3, and (d) NU-901. The false colors in the images depicting the variation in spatial lifetime distribution. (iii) The lifetime histrograms of (a) NU-1000-1, (b) NU-1000-2, (c) NU-1000-3, and (d) NU-901. The data were obtained from the three distinct regions (A, B, C) of the same crystal. The lifetime decay profiles were fitted using a three-exponential function. The figure was adapted with copyright permission from ref. no. 107. Copyright American Chemical Society.

structure were established using FLIM.[94] In addition, the dynamic processes within MOFs, such as the diffusion of guest molecules, chemical reactions, or changes in the framework structure are also monitored.[153] FLIM allows to capture of these processes in real time, providing a deeper understanding of the behavior of MOFs under various conditions. Furthermore, FLIM can also be used to create spatial maps of fluorescence lifetimes within a MOF sample. This can reveal heterogeneities in the sample, such as variations in pore sizes, defects, or differences in chemical composition across the MOF structure.[94,107,153]

Chen *et al*. used FLIM to elucidate the presence of polymorph in a series of Zr-based metal-organic frameworks (MOFs, Figure 15).[107] The MOF, namely NU-1000, consisted of Zr_6-based nodes and emissive pyrene-based linkers (Figure 15 ia, b). The irregularity in the crystal structure was thought to be due to the presence of the NU-901 phase. To investigate the fact, NU-1000-1, NU-1000-2, NU-1000-3, and NU-901 MOFs were synthesized. The microcrystals of the MOFs were used for the FLIM imaging to decipher the heterogeneity and the presence of different phases in the crystals.[107]

Figure 15 iia-d shows the FLIM images of the MOF crystals of NU-1000-1 (a), NU-1000-2 (b), NU-1000-3 (c), and NU-901 (d). The false colors in the images depicted the spatial distribution of the average fluorescence lifetime. The lifetime histograms at different points (A, B, C) in the same crystal are shown in Figure 15 iiia-d. Both NU-1000-1 and NU-901 showed almost the same average fluorescence lifetime in all the regions of the crystal. The result ascertained the phase purity of both crystals. NU-1000-2 also exhibited a nearly uniform lifetime distribution. Whereas NU-1000-3 showed a different lifetime distribution in all the points of the crystal indicating the phase impurity. The longitudinal center of the crystal exhibited lifetime distribution like NU-901. The result indicated the presence of a polymorph of phase NU-901 in NU-1000-3 MOF.[107]

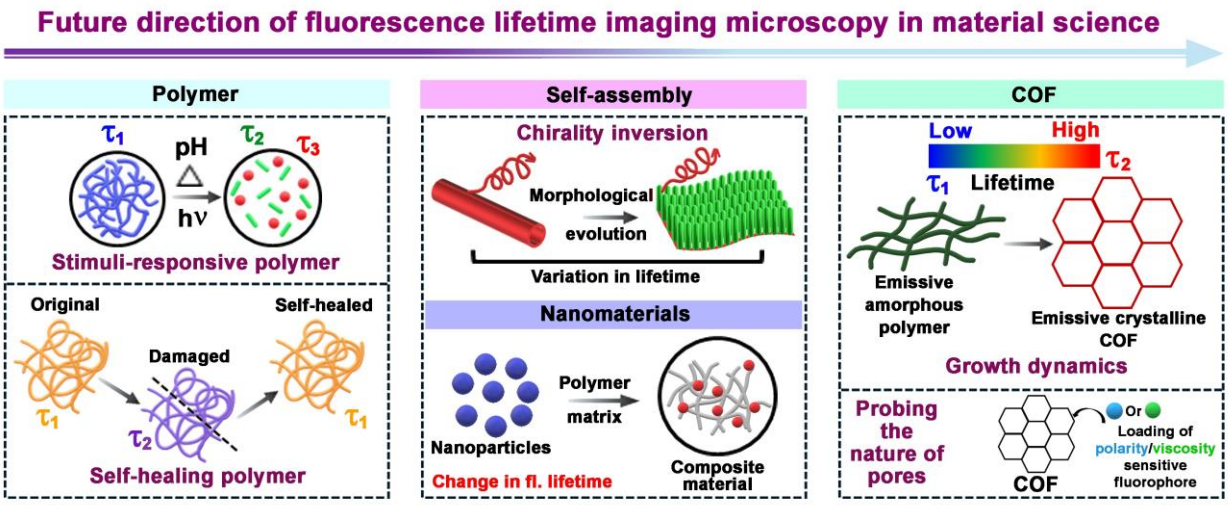

Figure 16. Schematic illustration depicting the future directions of fluorescence lifetime imaging microscopy in materials science research.

7. CONCLUSION AND OUTLOOK

We have highlighted the recent advancements in the application of FLIM for investigating the unique properties of various materials, including semiconductor nanocrystals, molecular self-assemblies, polymers, and metal-organic frameworks (MOFs). The significance of FLIM in understanding exciton dynamics and single-photon emission properties in semiconductor nanocrystals has been demonstrated. Its utility in unraveling the *in situ* molecular self-assembly process and probing stimuli-responsive morphological transformations has also been emphasized. Furthermore, FLIM has proven to be a vital complementary imaging technique for exploring the intricate structure-property relationships in polymers and MOFs. Thus, FLIM is poised to play an increasingly significant role in material science, especially as the demand for advanced materials with precise functional properties continues to grow. The future of FLIM in material science is marked by several promising prospects:

7.1. POLYMER:

FLIM will be essential in characterizing polymers that are sensitive to external stimuli like heat, pH, light, and mechanical stress (Figure 16). The ability to visualize and map the dynamic changes by fluorescence lifetime in real-time will help to understand and optimize the responsiveness of these materials. Imato *et al*. showed the polarity-induced photoswitching of spiropyran-based polymer. The use of FLIM for such types of polymeric systems can provide information about the influence of the microenvironment on the reversible photoswitching process.[154] Kumar *et al*. probed the kinetics of enzymatic hydrolysis for supramolecular polymer using circular dichroism. FLIM can be used as a complementary to explore the effect of the microenvironment on the hydrolysis process.[155] In addition, FLIM could be employed to monitor the healing process in self-repairing polymers. By mapping changes in fluorescence lifetime during the healing process, one can get more information into the molecular mechanisms that drive self-repair, leading to the development of more efficient self-healing systems (Figure 16). Peng *et al*. developed self-healing elastomers through kinetically controlled copolymerization. The incorporation of task-specific fluorescent dyes in the polymeric backbone can help to understand the kinetics of the self-healing process using FLIM.[156]

7.2. NANOMATERIAL:

FLIM can be beneficial to study nanocomposites and nanostructured materials, where understanding interactions at the nanoscale is key to optimizing material properties. FLIM can also be used to study the distribution and interaction of nanoparticles within polymer matrices (Figure 16). This is critical for developing advanced nanocomposites with tailored optical, electrical, and mechanical properties.

In addition, FLIM can be employed to explore ultrafast exciton dynamics in QDs and PNCs, providing an understanding of charge carrier recombination, and multi-exciton

interactions. The $g^{(2)}(0)$ value has been used to confirm whether a system is a single photon emitter or not. However, a multi-order correlation (third, fourth, and so on) can be helpful to exactly measure the multiexciton generation. A successful attempt has been made to calculate a third-order correlation curve by tuning the delay time between two pulses in a very recent study.[157] Integrating FLIM with multi-modal imaging and computational modeling can further bridge the gap between nanomaterial synthesis and their real-world applications in advanced technologies. These future directions underscore FLIM's potential as a transformative tool in semiconductor nanocrystal research.

7.3. MOLECULAR SELF-ASSEMBLY:

FLIM can be used to study exciton dynamics in self-assembled systems designed for optoelectronic applications, like organic photovoltaics or light-emitting diodes. The variation of fluorescence lifetime can be useful to demonstrate the exciton diffusion, recombination, and quenching processes, which are critical for optimizing the efficiency of these materials. Many self-assembled systems involve hierarchical organization where smaller building blocks form larger and more complex chiral structures. FLIM can provide insights into each level of this hierarchy, revealing how interactions at the molecular level influence the formation and stability of larger structures (Figure 16). Albertazzi *et al*. used stochastic optical reconstruction microscopy to demonstrate the monomer exchange during supramolecular polymerization. FLIM can be utilized in the future to explore microenvironment-sensitive similar kinds of dynamic molecular self-assembly processes.[158]

7.4. COVALENT ORGANIC FRAMEWORK:

To date, there are no reports to explore the salient features of covalent organic frameworks using FLIM. However, we strongly believe that FLIM can also be used to map the fluorescence lifetime of molecules within the pores of COFs (Figure 16). Since the fluorescence lifetime is influenced by the local environment, thus it can be beneficial to reveal the differences in pore polarity, the presence of guest molecules, or interactions between the framework and encapsulated species. This is crucial for optimizing COFs for applications like gas storage and separation. FLIM can be used to monitor the dynamics of guest molecules within COFs in real time. By observing changes in fluorescence lifetime, FLIM can be used to study the diffusion, binding, and release of molecules within the framework, which is essential for applications in catalysis, drug delivery, and sensing. Similarly, the growth and formation dynamics of fluorescent COF or fluorophore-tagged COFs can be probed using FLIM (Figure 16). Giri *et al*. demonstrated the molecular cage to COF transformation using both microscopic and spectroscopic techniques. In the future, the *in situ* incorporation of fluorescent dye in the pores of the COF can provide an in-depth understanding of dynamic covalent chemistry using FLIM.[159] Apart from a materialistic point of view, the following aspects of FLIM can be considered for the betterment of the field.

7.5. KEY DIRECTIONS:

1. The future will likely see an increase in the integration of FLIM with other imaging techniques, such as Raman spectroscopy, atomic force microscopy, and X-ray microscopy. This multimodal approach will provide a more comprehensive understanding of materials, correlating chemical, structural, and dynamic information. FLIM can also be combined with 3D imaging techniques, like confocal or multiphoton microscopy, to produce 3D maps of fluorescence lifetimes within materials. Also, 4D FLIM, which adds the temporal dimension to 3D imaging, could be used to study real-time dynamic processes.

2. The development of new fluorescent probes that are specifically tailored for material science applications can benefit the usage of FLIM. These probes will be designed to respond to specific environmental factors within materials, such as stress, strain, or chemical changes. There is also potential for the development of dyes with longer fluorescence lifetimes, which could improve the sensitivity and dynamic range of FLIM in material science applications.

Thus, the future of FLIM in material science is bright, with its potential applications expanding as technology continues to advance. Its ability to provide detailed, non-invasive, and real-time insights into material properties makes it an indispensable tool in the ongoing quest to develop

smarter, more efficient, and more sustainable materials.

AUTHOR INFORMATION

Corresponding Author

Subhankar Kundu. Research Division, Hoxworth Blood Center, College of Medicine, UC Health, University of Cincinnati, 3130 Highland Ave, Cincinnati, Ohio 45219. Email: kundusr@ucmail.uc.edu. orcid.org/0000-0001-9294-5551.

Fariyad Ali. Department of Chemistry, Iowa State University, 1605 Gilman Hall, Ames, Iowa. Email: Fariyadali46@gmail.com. orcid.org/0000-0003-1342-354X.

Author Contributions

‡These authors contributed equally.

Notes

The authors declare no competing financial interest.

ACKNOWLEDGMENT

We thank Mr. Subhadeep Das and Ms. Madhurima Sarkar for carefully reading and providing suggestions for the manuscript.

REFERENCES

1. Whitesides, G. M.; Grzybowski, B., Self-Assembly at All Scales. *Science* **2002,** *295* (5564), 2418-2421.
2. George, S. J.; de Bruijn, R.; Tomović, Ž.; Van Averbeke, B.; Beljonne, D.; Lazzaroni, R.; Schenning, A. P. H. J.; Meijer, E. W., Asymmetric Noncovalent Synthesis of Self-Assembled One-Dimensional Stacks by a Chiral Supramolecular Auxiliary Approach. *J. Am. Chem. Soc.* **2012,** *134* (42), 17789-17796.
3. Jalani, K.; Dhiman, S.; Jain, A.; George, S. J., Temporal switching of an amphiphilic self-assembly by a chemical fuel-driven conformational response. *Chem. Sci.* **2017,** *8* (9), 6030-6036.
4. Yuan, Z.; Zhou, C.; Tian, Y.; Shu, Y.; Messier, J.; Wang, J. C.; van de Burgt, L. J.; Kountouriotis, K.; Xin, Y.; Holt, E.; Schanze, K.; Clark, R.; Siegrist, T.; Ma, B., One-dimensional organic lead halide perovskites with efficient bluish white-light emission. *Nat. Commun.* **2017,** *8* (1), 14051.
5. Roy, B.; Reddy, M. C.; Hazra, P., Developing the structure–property relationship to design solid state multi-stimuli responsive materials and their potential applications in different fields. *Chem. Sci.* **2018,** *9* (14), 3592-3606.
6. Sedgwick, A. C.; Wu, L.; Han, H.-H.; Bull, S. D.; He, X.-P.; James, T. D.; Sessler, J. L.; Tang, B. Z.; Tian, H.; Yoon, J., Excited-state intramolecular proton-transfer (ESIPT) based fluorescence sensors and imaging agents. *Chem. Soc. Rev.* **2018,** *47* (23), 8842-8880.
7. Kundu, S.; Sk, B.; Pallavi, P.; Giri, A.; Patra, A., Molecular Engineering Approaches Towards All-Organic White Light Emitting Materials. *Chem. Eur. J.* **2020,** *26* (25), 5557-5582.
8. Wang, R.; Chen, C.; Zheng, Y.; Wang, H.; Liu, J.-W.; Yu, S.-H., Structure–property relationship of assembled nanowire materials. *Mater. Chem. Front.* **2020,** *4* (10), 2881-2903.
9. Hecht, M.; Würthner, F., Supramolecularly Engineered J-Aggregates Based on Perylene Bisimide Dyes. *Acc. Chem. Res.* **2021,** *54* (3), 642-653.
10. Jaiswal, S.; Das, S.; Kundu, S.; Rawal, I.; Anand, P.; Patra, A., Progress and perspectives: fluorescent to long-lived emissive multifunctional probes for intracellular sensing and imaging. *J. Mater. Chem. C* **2022,** *10* (16), 6141-6195.
11. Kundu, S.; Das, S.; Jaiswal, S.; Patra, A., Molecular to Supramolecular Self-Assembled Luminogens for Tracking the Intracellular Organelle Dynamics. *ACS Appl. Bio Mater.* **2022,** *5* (8), 3623-3648.
12. Park, H.; Kang, Y.; Kim, J., Enhancing Structure–Property Relationships in Porous Materials through Transfer Learning and Cross-Material Few-Shot Learning. *ACS Appl. Mater. Interfaces* **2023,** *15* (48), 56375-56385.
13. Qiu, S.; Zhang, D.; Yeddu, V.; Cordoba, C.; Blackburn, A. M.; Iosub, V.; Saidaminov, M. I., The Importance of Synthesis Conditions: Structure–Processing–Property Relationships. *J. Chem. Edu.* **2023,** *100* (2), 828-834.
14. Das, S.; Kundu, S.; Sk, B.; Sarkar, M.; Patra, A., Red Thermally Activated Delayed Fluorescence in Dibenzopyridoquinoxaline-Based Nanoaggregates. *Org. Mater.* **2021,** *3* (04), 477-487.
15. Kundu, S.; Behera, B.; Giri, A.; Saha, N.; Patra, A., N,N′-bicarbazole-benzothiadiazole-based conjugated porous organic polymer for reactive oxygen species generation in live cells. *Chem. Commun.* **2021,** *57* (56), 6875-6878.
16. Sk, B.; Sharma, S.; James, A.; Kundu, S.; Patra, A., N-Rich electron acceptors: triplet harvesting in multichromophoric pyridoquinoxaline and pyridopyrazine-based organic emitters. *J. Mater. Chem. C* **2020,** *8* (37), 12943-12950.
17. Hande, P. E.; Mishra, M.; Ali, F.; Kapoor, S.; Datta, A.; Gharpure, S. J., Design and Expeditious Synthesis of Quinoline-Pyrene-Based Ratiometric Fluorescent Probes for Targeting Lysosomal pH. *ChemBioChem* **2020,** *21* (10), 1492-1498.
18. Ajayaghosh, A.; George, S. J., First Phenylenevinylene Based Organogels: Self-Assembled Nanostructures via Cooperative Hydrogen Bonding and π-Stacking. *J. Am. Chem. Soc.* **2001,** *123* (21), 5148-5149.
19. An, B.-K.; Lee, D.-S.; Lee, J.-S.; Park, Y.-S.; Song, H.-S.; Park, S. Y., Strongly Fluorescent Organogel System Comprising Fibrillar Self-Assembly of a Trifluoromethyl-Based Cyanostilbene Derivative. *J. Am. Chem. Soc.* **2004,** *126* (33), 10232-10233.
20. Bandyopadhyay, S.; Kundu, S.; Giri, A.; Patra, A., A smart photosensitizer based on a red emitting solution processable porous polymer: generation of reactive oxygen species. *Chem. Commun.* **2018,** *54* (66), 9123-9126.
21. Chakrabarty, R.; Mukherjee, P. S.; Stang, P. J., Supramolecular Coordination: Self-Assembly of Finite Two- and Three-Dimensional Ensembles. *Chem. Rev.* **2011,** *111* (11), 6810-6918.
22. Cheng, H.-B.; Li, Y.; Tang, B. Z.; Yoon, J., Assembly strategies of organic-based imaging agents for fluorescence and photoacoustic bioimaging applications. *Chem. Soc. Rev.* **2020,** *49* (1), 21-31.
23. Chi, X.; Zhang, H.; Vargas-Zúñiga, G. I.; Peters, G. M.; Sessler, J. L., A Dual-Responsive Bola-Type Supra-amphiphile Constructed from a Water-Soluble Calix[4]pyrrole and a Tetraphenylethene-Containing Pyridine Bis-N-oxide. *J. Am. Chem. Soc.* **2016,** *138* (18), 5829-5832.
24. Dutta, T. K.; Das, S.; Sarkar, M.; Bhattacharjee, M.; Patra, A., Multistate Electrochromic Covalent Organic Framework Film for Electronic Safety Indicator. *Chem. Mater.* **2024,** *36* (16), 8027-8036.
25. Giri, A.; Khakre, Y.; Shreeraj, G.; Dutta, T. K.; Kundu, S.; Patra, A., The order–disorder conundrum: a trade-off between crystalline and amorphous porous organic polymers for task-specific applications. *J. Mater. Chem. A* **2022,** *10* (33), 17077-17121.
26. Hendricks, M. P.; Sato, K.; Palmer, L. C.; Stupp, S. I., Supramolecular Assembly of Peptide Amphiphiles. *Acc. Chem. Res.* **2017,** *50* (10), 2440-2448.
27. Kershaw, S. V.; Jing, L.; Huang, X.; Gao, M.; Rogach, A. L., Materials aspects of semiconductor nanocrystals for optoelectronic applications. *Mater. Horiz.* **2017,** *4* (2), 155-205.
28. Kumar, V.; Sk, B.; Kundu, S.; Patra, A., Dynamic and static excimer: a versatile platform for single component white-light emission and chelation-enhanced fluorescence. *J. Mater. Chem. C* **2018,** *6* (44), 12086-12094.
29. Lee, J.-S. M.; Cooper, A. I., Advances in Conjugated Microporous Polymers. *Chem. Rev.* **2020,** *120* (4), 2171-2214.

30. Lehn, J.-M., Supramolecular Chemistry—Scope and Perspectives Molecules, Supermolecules, and Molecular Devices (Nobel Lecture). *Angew. Chem. Int. Ed.* **1988,** *27* (1), 89-112.
31. Palmer, L. C.; Stupp, S. I., Molecular Self-Assembly into One-Dimensional Nanostructures. *Acc. Chem. Res.* **2008,** *41* (12), 1674-1684.
32. Patra, A.; Hebalkar, N.; Sreedhar, B.; Sarkar, M.; Samanta, A.; Radhakrishnan, T. P., Tuning the Size and Optical Properties in Molecular Nano/Microcrystals: Manifestation of Hierarchical Interactions. *Small* **2006,** *2* (5), 650-659.
33. Sarkar, M.; Sarkar, S.; Saha, M.; Luvani, K.; Patra, A., Intriguing Facets of Solution Processable Cross-Linked Porous Organic Polymers. *Acc. Chem. Res.* **2024,** *5* (11), 1353-1365.
34. Zou, R.; Wang, Q.; Wu, J.; Wu, J.; Schmuck, C.; Tian, H., Peptide self-assembly triggered by metal ions. *Chem. Soc. Rev.* **2015,** *44* (15), 5200-5219.
35. Abánades Lázaro, I.; Chen, X.; Ding, M.; Eskandari, A.; Fairen-Jimenez, D.; Giménez-Marqués, M.; Gref, R.; Lin, W.; Luo, T.; Forgan, R. S., Metal–organic frameworks for biological applications. *Nat. Rev. Methods Primers* **2024,** *4* (1), 42.
36. Kundu, S.; Das, S.; Dutta, A.; Patra, A., Three in One: Stimuli-Responsive Fluorescence, Solid-State Emission, and Dual-Organelle Imaging Using a Pyrene-Benzophenone Derivative. *The J. Phys. Chem. B* **2022,** *126* (3), 691-701.
37. Jaiswal, S.; Kundu, S.; Bandyopadhyay, S.; Patra, A., A hybrid upconversion nanoprobe for ratiometric detection of aliphatic biogenic amines in aqueous medium. *Nanoscale Adv.* **2021,** *3* (11), 3232-3239.
38. Jaiswal, S.; Pathak, J.; Kundu, S.; Patra, A., One-Pot Phosphine-Free Route for Single-Component White Light Emitting CdSexSy Alloy Nanocrystals. *ACS Sus. Chem. Eng.* **2021,** *9* (16), 5613-5622.
39. Kumar, B.; Rathnam, V. S. S.; Kundu, S.; Saxena, N.; Banerjee, I.; Giri, S., White-light-emitting NaYF4 Nanoplatform for NIR Upconversion-mediated Photodynamic Therapy and Bioimaging. *ChemNanoMat* **2018,** *4* (6), 583-595.
40. Kumar, V.; Kundu, S.; Sk, B.; Patra, A., A naked-eye colorimetric sensor for methanol and 'turn-on' fluorescence detection of Al3+. *New J. Chem.* **2019,** *43* (47), 18582-18589.
41. M, J. H.; Giri, A.; Kundu, S.; Kumar, V.; Sk, B.; Patra, A., Pyrene-cyanostyrene-pyridine triad: Multi-stimuli responsive fluorescent emitter and mitochondrial imaging. *Chem. Phys. Impact* **2021,** *3*, 100036.
42. Giri, A.; Biswas, S.; Hussain, M. D. W.; Dutta, T. K.; Patra, A., Nanostructured Hypercrosslinked Porous Organic Polymers: Morphological Evolution and Rapid Separation of Polar Organic Micropollutants. *ACS Appl. Mater. Interfaces* **2022,** *14* (5), 7369-7381.
43. Zhang, X.; Chen, Z.; Würthner, F., Morphology Control of Fluorescent Nanoaggregates by Co-Self-Assembly of Wedge- and Dumbbell-Shaped Amphiphilic Perylene Bisimides. *J. Am. Chem. Soc.* **2007,** *129* (16), 4886-4887.
44. Mitra, S.; Sasmal, H. S.; Kundu, T.; Kandambeth, S.; Illath, K.; Díaz Díaz, D.; Banerjee, R., Targeted Drug Delivery in Covalent Organic Nanosheets (CONs) via Sequential Postsynthetic Modification. *J. Am. Chem. Soc.* **2017,** *139* (12), 4513-4520.
45. Kubota, R.; Nakamura, K.; Torigoe, S.; Hamachi, I., The Power of Confocal Laser Scanning Microscopy in Supramolecular Chemistry: In situ Real-time Imaging of Stimuli-Responsive Multicomponent Supramolecular Hydrogels. *ChemistryOpen* **2020,** *9* (1), 67-79.
46. Venugopal, A.; Ruiz-Perez, L.; Swamynathan, K.; Kulkarni, C.; Calò, A.; Kumar, M., Caught in Action: Visualizing Dynamic Nanostructures Within Supramolecular Systems Chemistry. *Angew. Chem. Int. Ed.* **2023,** *62* (8), e202208681.
47. Banerjee, S.; Yang, R.; Courchene, C. E.; Conners, T. E., Scanning Electron Microscopy Measurements of the Surface Roughness of Paper. *Ind. Eng. Chem. Res.* **2009,** *48* (9), 4322-4325.
48. Meng, L.; Fonseca, J.; Sánchez-Naya, R.; Ghadiri, A. M.; Imaz, I.; Maspoch, D., Coassembly of Complementary Polyhedral Metal–Organic Framework Particles into Binary Ordered Superstructures. *J. Am. Chem. Soc.* **2024,** *146* (31), 21225-21230.
49. Polcari, D.; Dauphin-Ducharme, P.; Mauzeroll, J., Scanning Electrochemical Microscopy: A Comprehensive Review of Experimental Parameters from 1989 to 2015. *Chem. Rev.* **2016,** *116* (22), 13234-13278.
50. Srinivasan, C.; Mullen, T. J.; Hohman, J. N.; Anderson, M. E.; Dameron, A. A.; Andrews, A. M.; Dickey, E. C.; Horn, M. W.; Weiss, P. S., Scanning Electron Microscopy of Nanoscale Chemical Patterns. *ACS Nano* **2007,** *1* (3), 191-201.
51. Woodward, J. D.; Wepf, R. A., Three-Dimensional Field-Emission Scanning Electron Microscopy as a Tool for Structural Biology. In *Biological Field Emission Scanning Electron Microscopy*, 2019; pp 567-587.
52. Wang, Z. L., Transmission Electron Microscopy of Shape-Controlled Nanocrystals and Their Assemblies. *The J. Phys. Chem. B* **2000,** *104* (6), 1153-1175.
53. Franken, L. E.; Grünewald, K.; Boekema, E. J.; Stuart, M. C. A., A Technical Introduction to Transmission Electron Microscopy for Soft-Matter: Imaging, Possibilities, Choices, and Technical Developments. *Small* **2020,** *16* (14), 1906198.
54. Kubota, R.; Tanaka, W.; Hamachi, I., Microscopic Imaging Techniques for Molecular Assemblies: Electron, Atomic Force, and Confocal Microscopies. *Chem. Rev.* **2021,** *121* (22), 14281-14347.
55. Rizvi, A.; Mulvey, J. T.; Carpenter, B. P.; Talosig, R.; Patterson, J. P., A Close Look at Molecular Self-Assembly with the Transmission Electron Microscope. *Chem. Rev.* **2021,** *121* (22), 14232-14280.
56. Saha, A.; Nia, S. S.; Rodríguez, J. A., Electron Diffraction of 3D Molecular Crystals. *Chem. Rev.* **2022,** *122* (17), 13883-13914.
57. Chao, H.-Y.; Venkatraman, K.; Moniri, S.; Jiang, Y.; Tang, X.; Dai, S.; Gao, W.; Miao, J.; Chi, M., In Situ and Emerging Transmission Electron Microscopy for Catalysis Research. *Chem. Rev.* **2023,** *123* (13), 8347-8394.
58. Han, Y.; Wang, L.; Cao, K.; Zhou, J.; Zhu, Y.; Hou, Y.; Lu, Y., In Situ TEM Characterization and Modulation for Phase Engineering of Nanomaterials. *Chem. Rev.* **2023,** *123* (24), 14119-14184.
59. Li, G.; Zhang, H.; Han, Y., Applications of Transmission Electron Microscopy in Phase Engineering of Nanomaterials. *Chem. Rev.* **2023,** *123* (17), 10728-10749.
60. Moradifar, P.; Liu, Y.; Shi, J.; Siukola Thurston, M. L.; Utzat, H.; van Driel, T. B.; Lindenberg, A. M.; Dionne, J. A., Accelerating Quantum Materials Development with Advances in Transmission Electron Microscopy. *Chem. Rev.* **2023,** *123* (23), 12757-12794.
61. Kundu, S.; Chowdhury, A.; Nandi, S.; Bhattacharyya, K.; Patra, A., Deciphering the evolution of supramolecular nanofibers in solution and solid-state: a combined microscopic and spectroscopic approach. *Chem. Sci.* **2021,** *12* (16), 5874-5882.
62. García, R.; Magerle, R.; Perez, R., Nanoscale compositional mapping with gentle forces. *Nat. Mater.* **2007,** *6* (6), 405-411.
63. Krieg, M.; Fläschner, G.; Alsteens, D.; Gaub, B. M.; Roos, W. H.; Wuite, G. J. L.; Gaub, H. E.; Gerber, C.; Dufrêne, Y. F.; Müller, D. J., Atomic force microscopy-based mechanobiology. *Nat. Rev. Phys.* **2019,** *1* (1), 41-57.
64. Müller, D. J.; Dufrêne, Y. F., Atomic force microscopy as a multifunctional molecular toolbox in nanobiotechnology. *Nat. Nanotech.* **2008,** *3* (5), 261-269.
65. Ando, T.; Uchihashi, T.; Scheuring, S., Filming Biomolecular Processes by High-Speed Atomic Force Microscopy. *Chem. Rev.* **2014,** *114* (6), 3120-3188.
66. Fukui, T.; Uchihashi, T.; Sasaki, N.; Watanabe, H.; Takeuchi, M.; Sugiyasu, K., Direct Observation and Manipulation of Supramolecular Polymerization by High-Speed Atomic Force Microscopy. *Angew. Chem. Int. Ed.* **2018,** *57* (47), 15465-15470.
67. Shen, J.; Zhang, D.; Zhang, F.-H.; Gan, Y., AFM tip-sample convolution effects for cylinder protrusions. *Appl. Surf. Sci.* **2017,** *422*, 482-491.
68. Baggaley, E.; Botchway, S. W.; Haycock, J. W.; Morris, H.; Sazanovich, I. V.; Williams, J. A. G.; Weinstein, J. A., Long-lived metal complexes open up microsecond lifetime imaging microscopy

under multiphoton excitation: from FLIM to PLIM and beyond. *Chem. Sci.* **2014,** *5* (3), 879-886.

69. Becker, W.; Shcheslavskiy, V., *Fluorescence lifetime imaging with near-infrared dyes*. SPIE: 2013; Vol. 8588.

70. Berezin, M. Y.; Achilefu, S., Fluorescence Lifetime Measurements and Biological Imaging. *Chem. Rev.* **2010,** *110* (5), 2641-2684.

71. Datta, R.; Gillette, A.; Stefely, M.; Skala, M., Recent innovations in fluorescence lifetime imaging microscopy for biology and medicine. *J. Biomed. Opt.* **2021,** *26* (7), 070603.

72. Datta, R.; Heaster, T.; Sharick, J.; Gillette, A.; Skala, M., Fluorescence lifetime imaging microscopy: fundamentals and advances in instrumentation, analysis, and applications. *J. Biomed. Opt.* **2020,** *25* (7), 071203.

73. Easter, Q. T., Biopolymer hydroxyapatite composite materials: Adding fluorescence lifetime imaging microscopy to the characterization toolkit. *Nano Select* **2022,** *3* (4), 751-765.

74. Eivgi, O.; Ravenscroft, A. C.; Blum, S. A., Imaging Block-Selective Copolymer Solvation. *J. Am. Chem. Soc.* **2023,** *145* (4), 2058-2063.

75. Hirvonen, L. M.; Suhling, K., Fast Timing Techniques in FLIM Applications. *Front. in Phys.* **2020,** *8*.

76. Jahn, K.; Buschmann, V.; Hille, C., Simultaneous Fluorescence and Phosphorescence Lifetime Imaging Microscopy in Living Cells. *Sci. Rep.* **2015,** *5* (1), 14334.

77. Jana, S.; Nevskyi, O.; Höche, H.; Trottenberg, L.; Siemes, E.; Enderlein, J.; Fürstenberg, A.; Wöll, D., Local Water Content in Polymer Gels Measured with Super-Resolved Fluorescence Lifetime Imaging. *Angew. Chem. Int. Ed.* **2024,** *63* (10), e202318421.

78. Kuimova, M. K.; Yahioglu, G.; Levitt, J. A.; Suhling, K., Molecular Rotor Measures Viscosity of Live Cells via Fluorescence Lifetime Imaging. *J. Am. Chem. Soc.* **2008,** *130* (21), 6672-6673.

79. Kundu, S.; Das, S.; Patra, A., Fluorescence correlation spectroscopy and fluorescence lifetime imaging microscopy for deciphering the morphological evolution of supramolecular self-assembly. *Chem. Commun.* **2023,** *59* (52), 8017-8031.

80. Das, S.; Batra, A.; Kundu, S.; Sharma, R.; Patra, A., Unveiling autophagy and aging through time-resolved imaging of lysosomal polarity with a delayed fluorescent emitter. *Chem. Sci.* **2024,** *15* (1), 102-112.

81. Ahmed, T.; Seth, S.; Samanta, A., Mechanistic Investigation of the Defect Activity Contributing to the Photoluminescence Blinking of CsPbBr3 Perovskite Nanocrystals. *ACS Nano* **2019,** *13* (11), 13537-13544.

82. Singha, P. K.; Mukhopadhyay, T.; Tarif, E.; Ali, F.; Datta, A., Competition among recombination pathways in single FAPbBr3 nanocrystals. *The J. Chem. Phys.* **2024,** *161* (5).

83. Vishnu, E. K.; Kumar Nair, A. A.; Thomas, K. G., Core-Size-Dependent Trapping and Detrapping Dynamics in CdSe/CdS/ZnS Quantum Dots. *The J. Phys. Chem. C* **2021,** *125* (46), 25706-25716.

84. Rabouw, F. T.; Antolinez, F. V.; Brechbühler, R.; Norris, D. J., Microsecond Blinking Events in the Fluorescence of Colloidal Quantum Dots Revealed by Correlation Analysis on Preselected Photons. *The J. Phys. Chem. Lett.* **2019,** *10* (13), 3732-3738.

85. Yuan, G.; Gómez, D. E.; Kirkwood, N.; Boldt, K.; Mulvaney, P., Two Mechanisms Determine Quantum Dot Blinking. *ACS Nano* **2018,** *12* (4), 3397-3405.

86. Ali, F.; Das, S.; Banerjee, S.; Maddala, B. G.; Rana, G.; Datta, A., Intense photoluminescence from Cu-doped CdSe nanotetrapods triggered by ultrafast hole capture. *Nanoscale* **2021,** *13* (33), 14228-14235.

87. Ali, F.; Das, S.; Bhandari, P.; Datta, A., Mechanism of Enhancement of Stokes Shifted Photoluminescence Quantum Yield and Lifetime from Ag(I)-Doped CdSe Nanotetrapods: Implications for Optoelectronic and Photonic Devices. *ACS Appl. Nano Mater.* **2023,** *6* (8), 6670-6677.

88. Banerjee, S.; Maddala, B. G.; Ali, F.; Datta, A., Enhancement of the band edge emission of CdSe nano-tetrapods by suppression of surface trapping. *Phys. Chem. Chem. Phys.* **2019,** *21* (18), 9512-9519.

89. Das, S.; Rana, G.; Ali, F.; Datta, A., Single particle level dynamics of photoactivation and suppression of Auger recombination in aqueous Cu-doped CdS quantum dots. *Nanoscale* **2023,** *15* (9), 4469-4476.

90. Gogoi, H.; Maddala, B. G.; Ali, F.; Datta, A., Role of Solvent in Electron-Phonon Relaxation Dynamics in Core-Shell Au–SiO2 Nanoparticles. *ChemPhysChem* **2021,** *22* (21), 2201-2206.

91. Rana, G.; Das, S.; Singha, P. K.; Ali, F.; Maji, R.; Datta, A., The effect of Cu(I)-doping on the photoinduced electron transfer from aqueous CdS quantum dots. *The J. Chem. Phys.* **2024,** *161* (2).

92. Li, Q.; He, Y.; Chang, J.; Wang, L.; Chen, H.; Tan, Y.-W.; Wang, H.; Shao, Z., Surface-Modified Silicon Nanoparticles with Ultrabright Photoluminescence and Single-Exponential Decay for Nanoscale Fluorescence Lifetime Imaging of Temperature. *J. Am. Chem. Soc.* **2013,** *135* (40), 14924-14927.

93. López, P. A.; Blum, S. A., Fluorescence Lifetime Imaging Microscopy (FLIM) as a Tool to Understand Chemical Reactions and Catalysis. *ACS Catal.* **2024,** *14* (22), 17132-17147.

94. Schrimpf, W.; Jiang, J.; Ji, Z.; Hirschle, P.; Lamb, D. C.; Yaghi, O. M.; Wuttke, S., Chemical diversity in a metal–organic framework revealed by fluorescence lifetime imaging. *Nat. Commun.* **2018,** *9* (1), 1647.

95. Suhling, K.; Hirvonen, L. M.; Levitt, J. A.; Chung, P.-H.; Tregidgo, C.; Le Marois, A.; Rusakov, D. A.; Zheng, K.; Ameer-Beg, S.; Poland, S.; Coelho, S.; Henderson, R.; Krstajic, N., Fluorescence lifetime imaging (FLIM): Basic concepts and some recent developments. *Med. Photon.* **2015,** *27*, 3-40.

96. Terentyeva, T. G.; Hofkens, J.; Komatsuzaki, T.; Blank, K.; Li, C.-B., Time-Resolved Single Molecule Fluorescence Spectroscopy of an α-Chymotrypsin Catalyzed Reaction. *The J. Phys. Chem. B* **2013,** *117* (5), 1252-1260.

97. Woodcock, J. W.; Stranick, S. J.; Kotula, A. P.; Chen, S. H.; Engmann, S.; Gilman, J. W.; Holmes, G. A., Reaction-Induced structural and compositional heterogeneity in amine-cured epoxy/epoxy thermosets: Visualization of heterogeneity using fluorescence lifetime imaging microscopy (FLIM). *Polymer* **2023,** *273*, 125826.

98. Zhu, X.; Wang, X.; Zhang, H.; Zhang, F., Luminescence Lifetime Imaging Based on Lanthanide Nanoparticles. *Angew. Chem. Int. Ed.* **2022,** *61* (42), e202209378.

99. J. R. Lakowicz, Principles of Fluorescence Spectroscopy, Springer, New York, 2006.

100. Adhikari, M.; Houhou, R.; Hniopek, J.; Bocklitz, T., Review of Fluorescence Lifetime Imaging Microscopy (FLIM) Data Analysis Using Machine Learning. *J. Exp. Theo. Anal.* **2023,** *1* (1), 44-63.

101. Park, J.; Gao, L., Advancements in fluorescence lifetime imaging microscopy Instrumentation: Towards high speed and 3D. *Curr. Opin. Solid State and Mater. Science* **2024,** *30*, 101147.

102. Torrado, B.; Pannunzio, B.; Malacrida, L.; Digman, M. A., Fluorescence lifetime imaging microscopy. *Nat. Rev. Methods Primers* **2024,** *4* (1), 80.

103. Becker, L.; Janssen, N.; Layland, S. L.; Mürdter, T. E.; Nies, A. T.; Schenke-Layland, K.; Marzi, J., Raman Imaging and Fluorescence Lifetime Imaging Microscopy for Diagnosis of Cancer State and Metabolic Monitoring. *Cancers (Basel)* **2021,** *13* (22).

104. Fernandes, S.; Williams, E.; Finlayson, N.; Stewart, H.; Dhaliwal, C.; Dorward, D. A.; Wallace, W. A.; Akram, A. R.; Stone, J.; Dhaliwal, K.; Williams, G. O. S., Fibre-based fluorescence-lifetime imaging microscopy: a real-time biopsy guidance tool for suspected lung cancer. *Trans. Lung Cancer Research* **2024,** *13* (2), 355-361.

105. Ouyang, Y.; Liu, Y.; Wang, Z. M.; Liu, Z.; Wu, M., FLIM as a Promising Tool for Cancer Diagnosis and Treatment Monitoring. *Nano-Micro Lett.* **2021,** *13* (1), 133.

106. Siegel, J.; Elson, D. S.; Webb, S. E. D.; Benny Lee, K. C.; Vlandas, A.; Gambaruto, G. L.; Lévêque-Fort, S.; Lever, M. J.; Tadrous, P. J.; Stamp, G. W. H.; Wallace, A. L.; Sandison, A.; Watson, T. F.; Alvarez, F.; French, P. M. W., Studying biological tissue with fluorescence lifetime imaging: microscopy, endoscopy, and complex decay profiles. *Appl. Opt.* **2003,** *42* (16), 2995-3004.

107. Chen, X.; Jagadesan, P.; Valandro, S.; Hupp, J. T.; Schanze, K. S.; Goswami, S., Identifying the Polymorphs of Zr-Based Metal–Organic Frameworks via Time-Resolved Fluorescence Imaging. *ACS Mater. Lett.* **2022,** *4* (2), 370-377.

108. Kundu, S.; Sk, B.; Saha, N.; Das, S.; Dutta, T. K.; Batra, A.; Tomar, R. S.; Patra, A., Unraveling Molecular Assembly and Tracking Lipid Droplet Dynamics Using Fluorescent Phenanthroimidazole Derivatives. *ACS Mater. Lett.* **2023,** *5* (1), 27-35.

109. Ali, F.; Hande, P. E.; Kumar Sahoo, D.; Roy, R.; Gharpure, S. J.; Datta, A., Surfactant-induced fluorescence enhancement of a quinoline-coumarin derivative in aqueous solutions and dropcast films. *J. Photochem. Photobiol. A: Chem.* **2023,** *434*, 114209.

110. Wu, X.; Barner-Kowollik, C., Fluorescence-readout as a powerful macromolecular characterisation tool. *Chem. Sci.* **2023,** *14* (45), 12815-12849.

111. Wohlschläger, M.; Versen, M.; Löder, M. G. J.; Laforsch, C., Identification of different plastic types and natural materials from terrestrial environments using fluorescence lifetime imaging microscopy. *Anal. Bioanal. Chem.* **2024,** *416* (15), 3543-3554.

112. Malý, P.; Strachotová, D.; Holoubek, A.; Heřman, P., Interferometric excitation fluorescence lifetime imaging microscopy. *Nat. Commun.* **2024,** *15* (1), 8019.

113. Oleksiievets, N.; Mathew, C.; Thiele, J. C.; Gallea, J. I.; Nevskyi, O.; Gregor, I.; Weber, A.; Tsukanov, R.; Enderlein, J., Single-Molecule Fluorescence Lifetime Imaging Using Wide-Field and Confocal-Laser Scanning Microscopy: A Comparative Analysis. *Nano Lett.* **2022,** *22* (15), 6454-6461.

114. Oleksiievets, N.; Thiele, J. C.; Weber, A.; Gregor, I.; Nevskyi, O.; Isbaner, S.; Tsukanov, R.; Enderlein, J., Wide-Field Fluorescence Lifetime Imaging of Single Molecules. *The J. Phys. Chem. A* **2020,** *124* (17), 3494-3500.

115. Hu, F.; Zhang, H.; Sun, C.; Yin, C.; Lv, B.; Zhang, C.; Yu, W. W.; Wang, X.; Zhang, Y.; Xiao, M., Superior Optical Properties of Perovskite Nanocrystals as Single Photon Emitters. *ACS Nano* **2015,** *9* (12), 12410-12416.

116. Bera, S.; Tripathi, A.; Titus, T.; Sethi, N. M.; Das, R.; Afreen; Adarsh, K. V.; Thomas, K. G.; Pradhan, N., CsPbBr3 Perovskite Crack Platelet Nanocrystals and Their Biexciton Generation. *J. Am. Chem. Soc.* **2024,** *146* (29), 20300-20311.

117. Bose, R.; Zhou, X.; Guo, T.; Yang, H.; Yin, J.; Mishra, A.; Slinker, J. D.; Bakr, O. M.; Mohammed, O. F.; Malko, A. V., Single-Particle Spectroscopy as a Versatile Tool to Explore Lower-Dimensional Structures of Inorganic Perovskites. *ACS Ener. Lett.* **2021,** *6* (10), 3695-3708.

118. Panda, M. K.; Acharjee, D.; Mahato, A. B.; Ghosh, S., Facet Dependent Photoluminescence Blinking from Perovskite Nanocrystals. *Small* **2024,** *20* (33), 2311559.

119. Ahmed, T.; Paul, S.; Samanta, A., Photoluminescence Blinking Revealing Static and Dynamic Heterogeneity of the Hole Transfer Process in Phenothiazine-Adsorbed FAPbBr3 Single Nanocrystals. *The J. Phys. Chem. C* **2022,** *126* (21), 9109-9116.

120. Vishnu, E. K.; Thomas, E. M.; Prasad, L.; Thomas, K. G., Trap States in Semiconductor Quantum Dots: Friends or Foes. *The J. Phys. Chem. C* **2024,** *128* (11), 4373-4382.

121. Rainò, G.; Nedelcu, G.; Protesescu, L.; Bodnarchuk, M. I.; Kovalenko, M. V.; Mahrt, R. F.; Stöferle, T., Single Cesium Lead Halide Perovskite Nanocrystals at Low Temperature: Fast Single-Photon Emission, Reduced Blinking, and Exciton Fine Structure. *ACS Nano* **2016,** *10* (2), 2485-2490.

122. Yarita, N.; Tahara, H.; Ihara, T.; Kawawaki, T.; Sato, R.; Saruyama, M.; Teranishi, T.; Kanemitsu, Y., Dynamics of Charged Excitons and Biexcitons in CsPbBr3 Perovskite Nanocrystals Revealed by Femtosecond Transient-Absorption and Single-Dot Luminescence Spectroscopy. *The J. Phys. Chem. Lett.* **2017,** *8* (7), 1413-1418.

123. Gibson, N. A.; Koscher, B. A.; Alivisatos, A. P.; Leone, S. R., Excitation Intensity Dependence of Photoluminescence Blinking in CsPbBr3 Perovskite Nanocrystals. *The J. Phys. Chem. C* **2018,** *122* (22), 12106-12113.

124. Zhang, A.; Dong, C.; Ren, J., Tuning Blinking Behavior of Highly Luminescent Cesium Lead Halide Nanocrystals through Varying Halide Composition. *The J. Phys. Chem. C* **2017,** *121* (24), 13314-13323.

125. Seth, S.; Ahmed, T.; Samanta, A., Photoluminescence Flickering and Blinking of Single CsPbBr3 Perovskite Nanocrystals: Revealing Explicit Carrier Recombination Dynamics. *The J. Phys. Chem. Lett.* **2018,** *9* (24), 7007-7014.

126. Paul, S.; Samanta, A., Phase-Stable and Highly Luminescent CsPbI3 Perovskite Nanocrystals with Suppressed Photoluminescence Blinking. *The J. Phys. Chem. Lett.* **2022,** *13* (25), 5742-5750.

127. Paul, S.; Kishore, G.; Samanta, A., Photoluminescence Blinking of Quantum Confined CsPbBr3 Perovskite Nanocrystals: Influence of Size. *The J. Phys. Chem. C* **2023,** *127* (21), 10207-10214.

128. Galland, C.; Ghosh, Y.; Steinbrück, A.; Sykora, M.; Hollingsworth, J. A.; Klimov, V. I.; Htoon, H., Two types of luminescence blinking revealed by spectroelectrochemistry of single quantum dots. *Nature* **2011,** *479* (7372), 203-207.

129. Zhou, X.; Bose, R.; Zhu, X.; Mehta, A.; Kim, M. J.; Malko, A. V., Highly Emissive Zero-Dimensional Cesium Lead Iodide Perovskite Nanocrystals with Thermally Activated Delayed Photoluminescence. *The J. Phys. Chem. Lett.* **2023,** *14* (12), 2933-2939.

130. Garai, A.; Vishnu, E. K.; Banerjee, S.; Nair, A. A. K.; Bera, S.; Thomas, K. G.; Pradhan, N., Vertex-Oriented Cube-Connected Pattern in CsPbBr3 Perovskite Nanorods and Their Optical Properties: An Ensemble to Single-Particle Study. *J. Am. Chem. Soc.* **2023,** *145* (25), 13989-13999.

131. Varghese P. , M.; Rajan, A.; Vishnu, E. K.; Titus, T.; Thomas, K. G., Optimizing Electron Delocalization in CdSe-CdS Heteronanostructures: Insights from Single-Particle Photoluminescence Studies. *The J. Phys. Chem. C* **2024,** *128* (26), 10945-10954.

132. Thomas, E. M.; Pradhan, N.; Thomas, K. G., Reasoning the Photoluminescence Blinking in CdSe–CdS Heteronanostructures as Stacking Fault-Based Trap States. *ACS Ener. Lett.* **2022,** *7* (8), 2856-2863.

133. Vonk, S. J. W.; Rabouw, F. T., Biexciton Blinking in CdSe-Based Quantum Dots. *The J. Phys. Chem. Lett.* **2023,** *14* (23), 5353-5361.

134. Titus, T.; Vishnu, E. K.; Garai, A.; Dutta, S. K.; Sandeep, K.; Shelke, A.; Ajithkumar, T. G.; Shaji, A.; Pradhan, N.; Thomas, K. G., Biexciton Emission in CsPbBr3 Nanocrystals: Polar Facet Matters. *Nano Lett.* **2024,** *24* (34), 10434-10442.

135. Fixler, D.; Nayhoz, T.; Ray, K., Diffusion Reflection and Fluorescence Lifetime Imaging Microscopy Study of Fluorophore-Conjugated Gold Nanoparticles or Nanorods in Solid Phantoms. *ACS Photon.* **2014,** *1* (9), 900-905.

136. Rakshit, S.; Das, S.; Poonia, P.; Maini, R.; Kumar, A.; Datta, A., White Light Generation from a Self-Assembled Fluorogen–Surfactant Composite Light Harvesting Platform. *The J. Phys. Chem. B* **2020,** *124* (34), 7484-7493.

137. Xie, Y.; Arno, M. C.; Husband, J. T.; Torrent-Sucarrat, M.; O'Reilly, R. K., Manipulating the fluorescence lifetime at the sub-cellular scale via photo-switchable barcoding. *Nat. Commun.* **2020,** *11* (1), 2460.

138. Mañas-Torres, M. C.; Gila-Vilchez, C.; González-Vera, J. A.; Conejero-Lara, F.; Blanco, V.; Cuerva, J. M.; Lopez-Lopez, M. T.; Orte, A.; Álvarez de Cienfuegos, L., In situ real-time monitoring of the mechanism of self-assembly of short peptide supramolecular polymers. *Mater. Chem. Front.* **2021,** *5* (14), 5452-5462.

139. Kistwal, T.; Rakshit, S.; Maini, R.; Kumar, A.; Datta, A., Microscopic Insights into the Mechanism of White Light Generation by Disruptive Interaction between Human Serum Albumin Amyloid Fibrils and Surfactant-AIEgen Nanorods. *The J. Phys. Chem. Lett.* **2022,** *13* (31), 7355-7362.

140. Rakshit, S.; Das, S.; Govindaraj, V.; Maini, R.; Kumar, A.; Datta, A., Morphological Evolution of Strongly Fluorescent Water Soluble AIEEgen-Triblock Copolymer Mixed Aggregates with Shape-Dependent Cell Permeability. *The J. Phys. Chem. B* **2020,** *124* (45), 10282-10291.

141. Mei, J.; Leung, N. L. C.; Kwok, R. T. K.; Lam, J. W. Y.; Tang, B. Z., Aggregation-Induced Emission: Together We Shine, United We Soar! *Chem. Rev.* **2015,** *115* (21), 11718-11940.
142. Burke, S. E.; Eisenberg, A., Kinetics and Mechanisms of the Sphere-to-Rod and Rod-to-Sphere Transitions in the Ternary System PS310-b-PAA52/Dioxane/Water. *Langmuir* **2001,** *17* (21), 6705-6714.
143. Zhang, J.; Xu, B.; Tian, W.; Xie, Z., Tailoring the morphology of AIEgen fluorescent nanoparticles for optimal cellular uptake and imaging efficacy. *Chem. Sci.* **2018,** *9* (9), 2620-2627.
144. Wang, M.; Xu, Y.; Liu, Y.; Gu, K.; Tan, J.; Shi, P.; Yang, D.; Guo, Z.; Zhu, W.; Guo, X.; Cohen Stuart, M. A., Morphology Tuning of Aggregation-Induced Emission Probes by Flash Nanoprecipitation: Shape and Size Effects on in Vivo Imaging. *ACS Appl. Mater. Interfaces* **2018,** *10* (30), 25186-25193.
145. Liu, J.; Liu, Z.; Mi, F.; Yao, Z.; Fang, X.; Wang, Y.; Zhao, Z.; Wu, C., Fluorescence Lifetime Multiplex Imaging in Expansion Microscopy with Tunable Donor–Acceptor Polymer Dots. *Chem. Biomed. Imaging* **2023,** *1* (6), 550-557.
146. Orte, A.; Alvarez-Pez, J. M.; Ruedas-Rama, M. J., Fluorescence Lifetime Imaging Microscopy for the Detection of Intracellular pH with Quantum Dot Nanosensors. *ACS Nano* **2013,** *7* (7), 6387-6395.
147. Petrášek, Z.; Bolivar, J. M.; Nidetzky, B., Confocal Luminescence Lifetime Imaging with Variable Scan Velocity and Its Application to Oxygen Sensing. *Anal. Chem.* **2016,** *88* (21), 10736-10743.
148. Eivgi, O.; Blum, S. A., Real-Time Polymer Viscosity–Catalytic Activity Relationships on the Microscale. *J. Am. Chem. Soc.* **2022,** *144* (30), 13574-13585.
149. Grecco, H. E.; Roda-Navarro, P.; Girod, A.; Hou, J.; Frahm, T.; Truxius, D. C.; Pepperkok, R.; Squire, A.; Bastiaens, P. I. H., In situ analysis of tyrosine phosphorylation networks by FLIM on cell arrays. *Nat. Methods* **2010,** *7* (6), 467-472.
150. Long, Y.; Stahl, Y.; Weidtkamp-Peters, S.; Postma, M.; Zhou, W.; Goedhart, J.; Sánchez-Pérez, M.-I.; Gadella, T. W. J.; Simon, R.; Scheres, B.; Blilou, I., In vivo FRET–FLIM reveals cell-type-specific protein interactions in Arabidopsis roots. *Nature* **2017,** *548* (7665), 97-102.
151. Peacock, H.; Blum, S. A., Surfactant Micellar and Vesicle Microenvironments and Structures under Synthetic Organic Conditions. *J. Am. Chem. Soc.* **2023,** *145* (13), 7648-7658.
152. Garcia, A. I. V.; Blum, S. A., Polymer Molecular Weight Determination via Fluorescence Lifetime. *J. Am. Chem. Soc.* **2022,** *144* (49), 22416-22420.
153. Schrimpf, W.; Ossato, G.; Hirschle, P.; Wuttke, S.; Lamb, D. C., Investigation of the Co-Dependence of Morphology and Fluorescence Lifetime in a Metal-Organic Framework. *Small* **2016,** *12* (27), 3651-3657.
154. Imato, K.; Momota, K.; Kaneda, N.; Imae, I.; Ooyama, Y., Photoswitchable Adhesives of Spiropyran Polymers. *Chem. Mater.* **2022,** *34* (18), 8289-8296.
155. Kumar, M.; Brocorens, P.; Tonnelé, C.; Beljonne, D.; Surin, M.; George, S. J., A dynamic supramolecular polymer with stimuli-responsive handedness for in situ probing of enzymatic ATP hydrolysis. *Nat. Commun.* **2014,** *5* (1), 5793.
156. Peng, Y.; Zhao, L.; Yang, C.; Yang, Y.; Song, C.; Wu, Q.; Huang, G.; Wu, J., Super tough and strong self-healing elastomers based on polyampholytes. *J. Mater. Chem. A* **2018,** *6* (39), 19066-19074.
157. Kazes, M.; Nakar, D.; Cherniukh, I.; Bodnarchuk, M. I.; Feld, L. G.; Zhu, C.; Amgar, D.; Rainò, G.; Kovalenko, M. V.; Oron, D., Observation of Three-Photon Cascaded Emission from Triexcitons in Giant CsPbBr3 Quantum Dots at Room Temperature. *Nano Lett.* **2024,** *24* (42), 13185-13191.
158. Albertazzi, L.; van der Zwaag, D.; Leenders, C. M. A.; Fitzner, R.; van der Hofstad, R. W.; Meijer, E. W., Probing Exchange Pathways in One-Dimensional Aggregates with Super-Resolution Microscopy. *Science* **2014,** *344* (6183), 491-495.
159. Giri, A.; Shreeraj, G.; Dutta, T. K.; Patra, A., Transformation of an Imine Cage to a Covalent Organic Framework Film at the Liquid–Liquid Interface. *Angew. Chem. Int. Ed.* **2023,** *62* (23), e202219083.